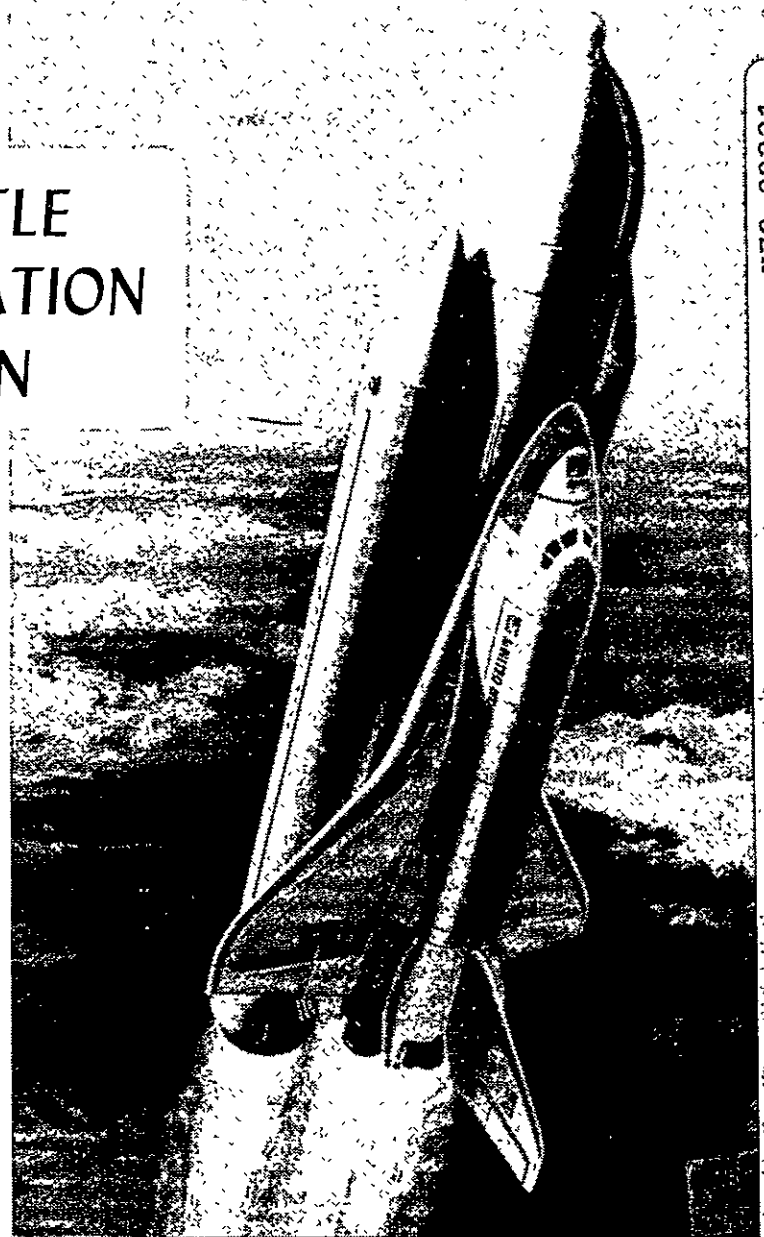


SPACE SHUTTLE PLUME/SIMULATION APPLICATION

FINAL SUMMARY REPORT



N79-29221
Unclas
G3/16 31706
(NASA-CR-161275) SPACE SHUTTLE
PLUME/SIMULATION APPLICATION Final Summary
Report (Northrop Services, Inc., Huntsville,
Ala.) 75 p. HC A04/NF A01
CSCL 20H

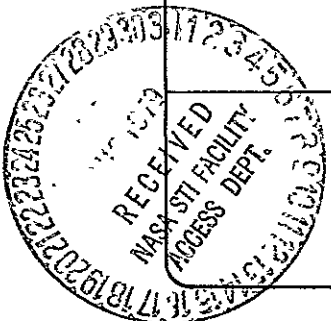
Prepared for:

**NATIONAL AERONAUTICS AND SPACE ADMINISTRATION
GEORGE C. MARSHALL SPACE FLIGHT CENTER
Science and Engineering Directorate
Under Contract NAS8-32524**

Prepared by:

NORTHROP SERVICES, INC.

P. O. Box 1484 Huntsville, Alabama 35807 (205) 837-0580



**SPACE SHUTTLE PLUME SIMULATION APPLICATION
FINAL SUMMARY REPORT**

15 May 1979

by



W. Boyle
B. Conine
G. Bell

Prepared for:

**NATIONAL AERONAUTICS AND SPACE ADMINISTRATION
GEORGE C. MARSHALL SPACE FLIGHT CENTER
SCIENCE AND ENGINEERING DIRECTORATE**

Under Contract NAS8-32524

Reviewed and Approved by:

M.A. Sloan, Jr., Manager
Technology

**NORTHROP SERVICES, INC.
ENGINEERING AND TECHNOLOGY CENTER
P.O. BOX 1484
HUNTSVILLE, ALABAMA 35807
(205)837-0580**

FOREWORD

This document summarizes the results of data and data analysis of two wind tunnel test programs to define the plume induced environments on the Space Shuttle vehicle. The work was performed for the NASA Marshall Space Flight Center, Huntsville, Alabama. The NASA technical monitors for this study was Mssrs. Kenneth L. Blackwell and Joseph L. Simms of the Systems Dynamics Laboratory.

TABLE OF CONTENTS

<u>Section</u>	<u>Title</u>	<u>Page</u>
	FOREWORD.	ii
	LIST OF ILLUSTRATIONS.	iv
	LIST OF TABLES.	v
	GENERAL NOMENCLATURE.	vi
	TEST NOMENCLATURE	vii
	GAS DYNAMIC NOMENCLATURE.	ix
	REVISIONS	xi
I	INTRODUCTION.	1-1
II	WIND TUNNEL MODELS	2-1
III	TEST CONDITIONS	3-1
IV	WIND TUNNEL MODEL NOZZLE CALIBRATION ANALYSIS	4-1
V	PLUME SIMULATION.	5-1
VI	DATA ANALYSIS	6-1
VII	TEST RESULTS.	7-1
VIII	BASE MATH MODEL	8-1
IX	FOREBODY PLUME INDUCED MATH. MODEL	9-1
X	CONCLUSIONS	10-1
XI	RECOMMENDATIONS	11-1
XII	REFERENCES	12-1

LIST OF ILLUSTRATIONS

<u>Figure</u>	<u>Title</u>	<u>Page</u>
2-1	IA119 MODEL INSTALLATION.	2-3
2-2	FLOW THROUGH NOZZLE AIR SUPPLY STRUTS - IA119 MODEL	2-4
3-1	SCHEDULE 6 ELEVON DEFLECTIONS	3-2
3-2	ELEVON SCHEDULE	3-3
3-3	ELEVON SCHEDULE	3-4
3-4	ELEVON SCHEDULE	3-5
3-5	ELEVON SCHEDULE	3-6
3-6	ELEVON SCHEDULE	3-7
3-7	ELEVON DEFLECTION MATRIX ($M_{\infty} = 1.55$).	3-8
3-8	ELEVON DEFLECTION MATRIX ($M_{\infty} = 1.80$).	3-9
3-9	ELEVON DEFLECTION MATRIX ($M_{\infty} = 2.20$).	3-10
3-10	ELEVON DEFLECTION MATRIX ($M_{\infty} = 2.50$).	3-11
4-1	SSME NOZZLE CHAMBER TO EXIT PRESSURE RATIO - IA119.	4-2
4-2	SRB NOZZLE CHAMBER TO EXIT PRESSURE RATIO - IA119	4-3
4-3	SSME NOZZLE CHAMBER TO EXIT PRESSURE RATIO - IA138.	4-4
4-4	SRB NOZZLE CHAMBER TO EXIT PRESSURE RATIO - IA138	4-5
5-1	PROTOTYPE POSSIBILITY CURVE	5-3
5-2	SIMILARITY PARAMETER EXPONENT	5-4
5-3	PLUME FLOW FIELD AREAS.	5-5
6-1	PLUME FLOW FIELD AREAS.	6-4

LIST OF TABLES

<u>Table</u>	<u>Title</u>	<u>Page</u>
5-1	CORRELATION PARAMETERS.	5-6
8-1	BASE AXIAL FORCE COEFFICIENT.	8-5
8-2	BASE NORMAL FORCE COEFFICIENT	8-6
8-3	BASE PITCHING MOMENT COEFFICIENT.	8-7
8-4	BASE COEFFICIENT PARTIALS	8-8
8-5	BASE AXIAL FORCE (LBS).	8-9
8-6	BASE NORMAL FORCE (LBS)	8-10
8-7	BASE PITCHING MOMENT (FT. LBS)	8-11
8-8	BASE AXIAL FORCE PARTIALS	8-12
8-9	IA-119 BASE COEFFICIENT TOLERANCES.	8-13
8-10	BASE MOMENT INCREMENTS.	8-14
9-1	SSLV AND ORBITER POWER DELTA - NORMAL FORCE COEFFICIENT - FOREBODY.	9-5
9-2	VERTICAL TAIL SIDE FORCE POWER DELTA.	9-6
9-3	FOREBODY FORCE COEFFICIENT TOLERANCES - SSLV AND ELEMENTS.	9-7
9-4	FOREBODY MOMENT INCREMENT EQUATIONS - SSLV AND ELEMENTS .	9-8
9-5	FOREBODY FORCE TOLERANCES - COMPONENTS.	9-9
9-6	FOREBODY MOMENT EQUATIONS - COMPONENTS.	9-10

GENERAL NOMENCLATURE

SYMBOL	DEFINITION
ET	Space Shuttle external tank
O	Space Shuttle Orbiter
SRB	Space Shuttle Solid Rocket Booster
SSLV	Space Shuttle Launch Vehicle
Base	Locations on the Space Shuttle where the nozzle exhaust plumes are the primary influence in determining the local pressure environment
Components	Portions of the Orbiter; wing, body flap, etc.
Elements	Primary elements of the SSLV, Orbiter, ET, SRB's
Forebody	Locations on the Space Shuttle where the nozzle exhaust plumes are the secondary influence in determining the local pressure environments

TEST NOMENCLATURE

<u>Symbol</u>	<u>Definition</u>
<u>General:</u>	
C_A	Axial force coefficient
C_{BV}	Vertical tail bending moment coefficient
C_{BW}	Wing-root bending-moment coefficient
C_H	Hinge moment coefficient
C_{HEI}	Hinge-moment coefficient for inboard elevon.
C_{HEO}	Hinge-moment coefficient for outboard elevon.
C_l	Rolling moment coefficient
C_M	Pitching moment coefficient
C_N	Normal force coefficient
C_{NW}	Wing normal-force coefficient
C_{TV}	Vertical tail torsion moment coefficient
C_{TW}	Wing-root torsion-moment coefficient
C_Y	Side force coefficient
C_{YN}	Yawing moment coefficient
C_{YV}	Vertical tail shear force coefficient
L	Reference length, in. or ft. defined in Table 6-10
S	Reference area, ft ² defined in Table 6-10

SUBSCRIPTS

B	Base
F	Forebody - fuselage
C_P	Determined using power on pressure coefficient
DEL	Determined using power-on minus power-off delta pressure coefficient
O	Orbiter



TEST NOMENCLATURE

ET

ET

SRB

SRB

PON

Power On

POF

Power Off

GAS DYNAMIC NOMENCLATURE

<u>Symbol</u>	<u>Definition</u>
P_i	Pressure (absolute) at model surface tap i, psia
C_{P_i}	Pressure coefficient for model surface tap i.
ΔC_{P_i}	$C_{P_{\text{Power On}}} - C_{P_{\text{Power Off}}}$
P_{c_j}	Chamber pressure (absolute) for nozzle j, psia
P_{e_j}	Exit pressure (absolute) for nozzle j. psia
CPR_j	Chamber-pressure ratio for nozzle j
γ_j	Ratio of specific heats for nozzle J
$P_c/P_{\infty \text{ ORB}}$	SSME chamber to freestream pressure ratio
$P_c/P_{\infty \text{ SRB}}$	SRB chamber to freestream pressure ratio
P_c/P_e	Chamber to exit nozzle pressure ratio
P_c/P_{wall}	Chamber to nozzle wall pressure ratio
M_j	Plume boundary Mach number at nozzle lip
M_E	Nozzle exit Mach number at nozzle wall (inviscid)
N	Exponent of ratio of specific heats and in similarity parameters
δ_j	Initial plume expansion angle
<u>Deflections:</u>	
δ_{E_I}	Left inboard elevon setting, corrected for load deflection, deg.
δ_{E_O}	Left outboard elevon setting, corrected for load deflection, deg.
γ_{N_j}	Pitch-angle of nozzle-j axis in a plane parallel to the Orbiter plane-of-symmetry, deg.
γ_{N_j}	Pitch-angle of nozzle-j axis in a plane which yaws with the nozzle, deg.
ψ_{N_j}	Yaw-angle of nozzle-j axis in an Orbiter waterplane, deg.

Test Operations:

M	Freestream Mach number.
Re/ft	Freestream unit Reynolds number, ft ⁻¹ .
q	Freestream dynamic pressure, psf.
P _∞	Freestream static pressure, psia.
P _T	Freestream total pressure, psia.
T	Freestream static temperature, °R.
T _T	Freestream total temperature, °R.
α	Model angle-of-attack, deg.
β	Model angle-of-sideslip, deg.
T _T _{SRB}	SRB supply total temperature, °R.
T _T _{MPS}	MPS supply total temperature, °R.
P _C _{MPS}	MPS supply total pressure, psia.
P _C _{SRB}	SRB supply total pressure, psia.

REVISIONS			
REV SYM	DESCRIPTION	DATE	APPROVAL

Section I

INTRODUCTION

An analysis of pressure and strain-gage data from Space Shuttle wind tunnel test IA119 and IA138 was performed to define the influence on aerodynamic characteristics resulting from the main propulsion system (MPS) and solid rocket booster (SRB) plumes. Aerodynamic characteristics of each of the elements, the components and total vehicle of the Space Shuttle vehicle during ascent flight was to be considered.

Test IA119 was a transonic wind tunnel test of a 0.02 scale model of the Space Shuttle launch vehicle. The test was conducted in the 11 x 11-foot section of the NASA/AMES Research Center Unitary Plan Wind Tunnel. Pressure data were obtained over the aft portions of the space shuttle wind tunnel model in addition to wing and elevon gage data.

Test IA138 was a supersonic wind tunnel test of a 0.01-scale model of the Space Shuttle launch vehicle. The test was conducted in the 9 x 7-foot section of the NASA/AMES Research Center Unitary Plan Wind Tunnel. Pressure data were obtained over the aft portions of the space shuttle wind tunnel model. Wing and elevon gage data were also obtained.

The simulant gas used to develop the model exhaust plumes was air. A portion of the tests were devoted to testing at various power levels. Data from the power level portion was used in conjunction with prototype possibility curves to evaluate nominal power levels. The nominal power levels were used during the investigation of changes in model attitude, elevon deflections and nozzle gimbal angles on the aerodynamic characteristics. The simulation parameter used to develop nominal power levels was $[\delta_j \gamma_j^N]_{\text{PROT}} = [\delta_j \gamma_j^N]_{\text{MODEL}}$ where N varies with Mach number.

Aerodynamic loads induced by the plumes were developed for the Space Shuttle base areas and forebody areas. The base areas are, the orbiter base including nozzles, the ET base and the SRB base. The forebody includes those areas of the orbiter forward of the base. The forebody includes the body flap, the wings and elevons, and the ET and SRB areas forward of the base.

A math model of the plume induced aerodynamic characteristics designed to match the forebody aerodynamic math model was developed for a range of Mach numbers. The aerodynamic characteristics of the base are presented in terms of forces and moments versus attitude. The aerodynamic characteristics of the total vehicle base and forebody are presented in terms of aerodynamic coefficients for the range of Mach numbers from 0.6 to 2.5. Aerodynamic characteristics of the elements component base and vehicle forebody are presented for Mach numbers from 0.6 to 2.5. Aerodynamic characteristics are presented vs Mach numbers compatible with Mach numbers used in defining forebody aerodynamic characteristics.

Tolerance values were developed for all plume induced aerodynamic characteristics. The tolerance values were developed in terms of a math model and include simulation parameter uncertainties, model instrumentation uncertainties, model configuration uncertainties (including tunnel-model support interference uncertainties and Reynolds number effects).

The results of the above analysis and math model of the IA119 transonic data are presented in detail in reference 1. The result of the base pressure integration computer program, gage data, and plotted data are presented in the appendix to reference 1.

The results of the analysis and math model of the IA138 supersonic data are presented in reference 2. The results of the IA138 base pressure integration computer program, gage data, and plotted data are presented in the appendix to reference 2.

Brief discussions of the wind tunnel test programs, data analysis tasks and analysis procedures are presented in the following sections. Examples of the results and math models of the results are also presented.

Section II

WIND TUNNEL MODELS

The wind tunnel model used for the IA119 test was a .02 scale Space Shuttle Launch Vehicle configuration. The wind tunnel model is designated - 88 OTS Configuration 140C (modified) Jet - Plume Integrated Space Shuttle Vehicle. The wind tunnel model is essentially the same as was used for an earlier Space Shuttle plume test IA19, conducted in 1974. The major difference being that the contoured SSME flow through nozzles were used during the IA119 test and conical SSME nozzles were used during the IA19 test. The orbiter model was the 140C model configuration which generally represents the OV101 orbiter mold lines. The OV102 mold lines have significant differences in the canopy contour, the wing section near the glove-wing fairing, and the elevon contour. Details of the model configuration can be obtained from the pretest report (reference³).

The model was strut mounted as shown in Figure 2-1. Cold air was supplied through the strut to the SSME and SRB nozzles. An air supply strut was mounted between the ET and orbiter to supply air to the simulated SSME nozzles as shown in Figure 2-2. The SSME nozzles were contoured with an exit plane lip angle of 5 degrees. The SRB nozzles were conical with a lip angle of 27.5 degrees.

The left orbiter wing was strain-gage instrumented to obtain wing shear forces, root bending moments and torsion moments. The inboard and outboard elevons on the left wing were separately strain-gage instrumented to obtain hinge moments. The vertical tail was also strain-gage instrumented to obtain shear, bending moments, and torsion moments. The right orbiter wing and elevons were pressure instrumented. All base, nozzle, and portions of each element forebody area were pressure instrumented.

The flow through MPS nozzles and SRB nozzles were capable of being set at various gimbal-angle positions and several gimbal patterns were investigated. The inboard and outboard elevons were also capable of being set at various deflection angles and data were obtained for a series of elevon deflection combinations.

The wind tunnel model used for the IA138 test was a 0.01 scale space shuttle launch vehicle configuration. The wind tunnel model is designated - 75 OTS Configuration 140C (modified) Jet - Plume Integrated Space Shuttle Vehicle. The orbiter model was the 140C model configuration which generally represents the OV101 orbiter mold lines. The OV102 mold lines have significant differences in the canopy contour, the wing section near the glove-wing fairing, and the elevon contour. Details of the model configuration can be obtained from the pretest report (reference 4).

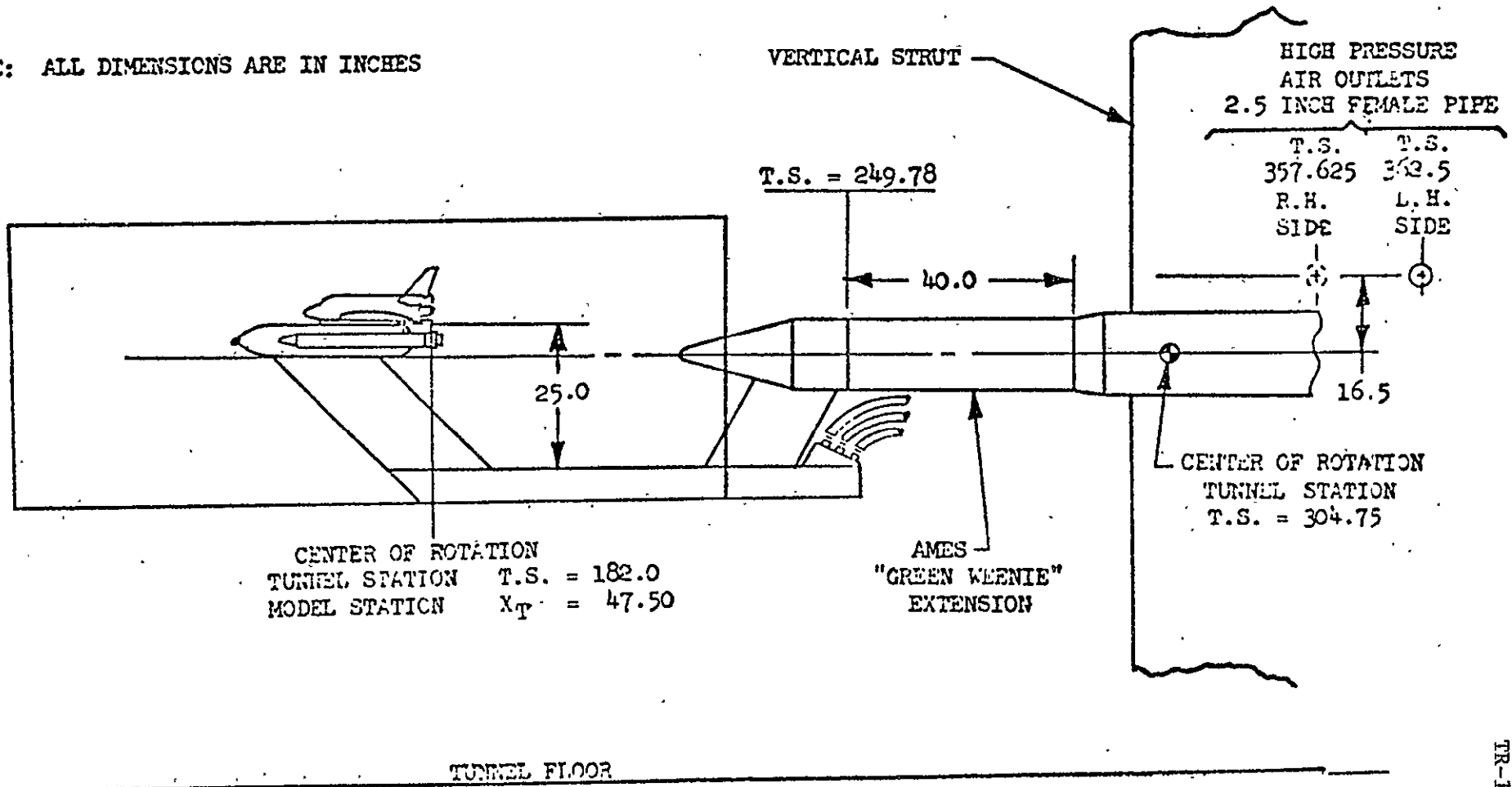
The model was strut mounted similar to the IA119 model as shown in Figure 2-1. Cold air was supplied through the strut to the SSME and SRB nozzles. An air supply strut was mounted between the ET and orbiter to supply air to the simulated SSME nozzles as shown in Figure 2-2. The SSME nozzles were conical with an exit plane lip angle of 11.0 degrees. The SRB nozzles were conical with a lip angle of 27.5 degrees.

A partial right orbiter wing was strain-gage instrumented to obtain wing shear forces, root bending moments and torsion moments. The inboard and outboard elevons on the left wing were also separately strain-gage instrumented to obtain hinge moments. All base, nozzle, and portions of each element forebody were pressure instrumented.

ARC UPWT - 11' x 11'
MODEL INSTALLATION

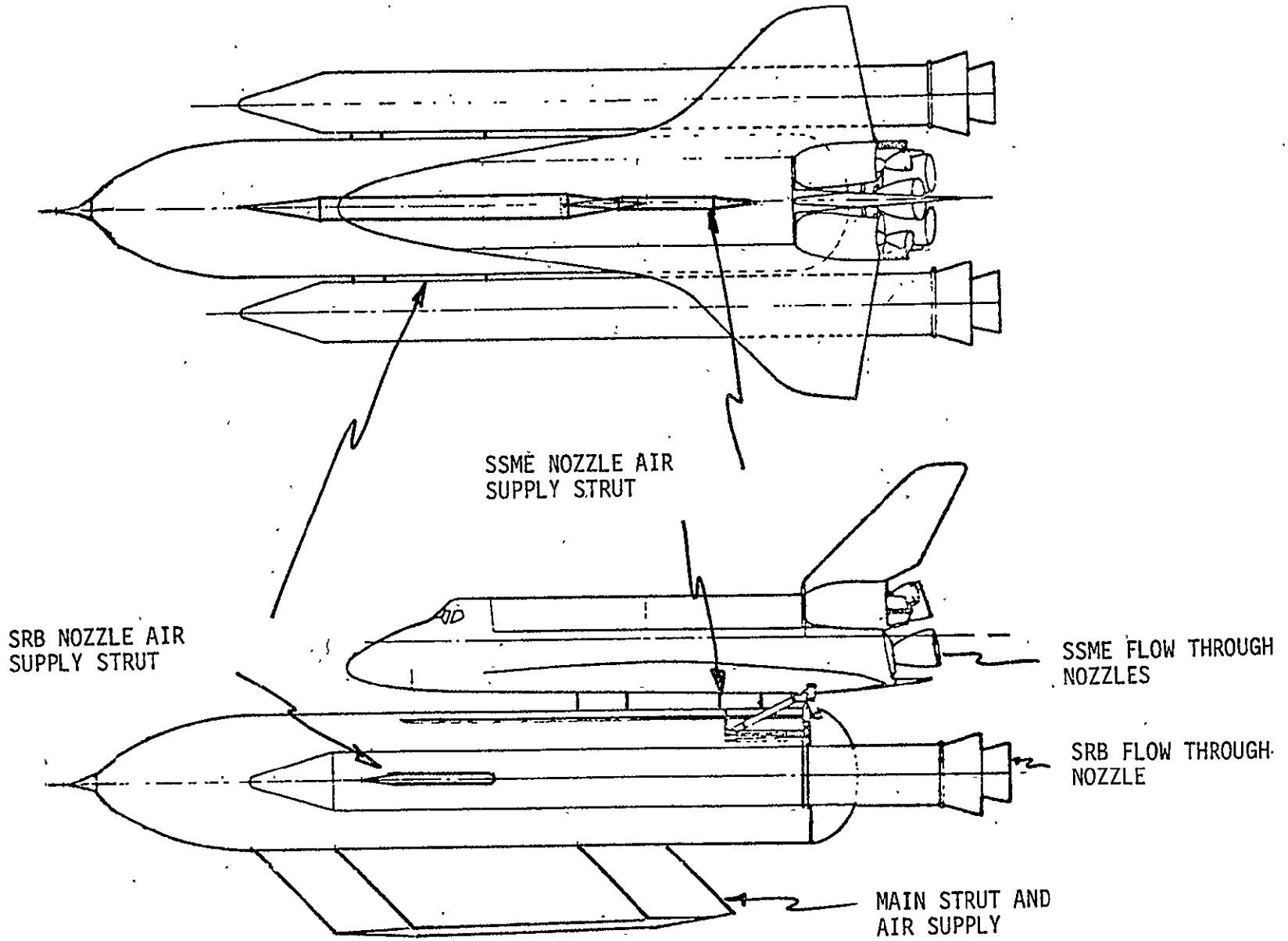
TUNNEL CEILING

NOTE: ALL DIMENSIONS ARE IN INCHES



2-3

Figure 2-1. IA119 MODEL INSTALLATION



2-4.

Figure 2-2. FLOW THROUGH NOZZLE AIR SUPPLY STRUTS -- IA119 MODEL

Section III

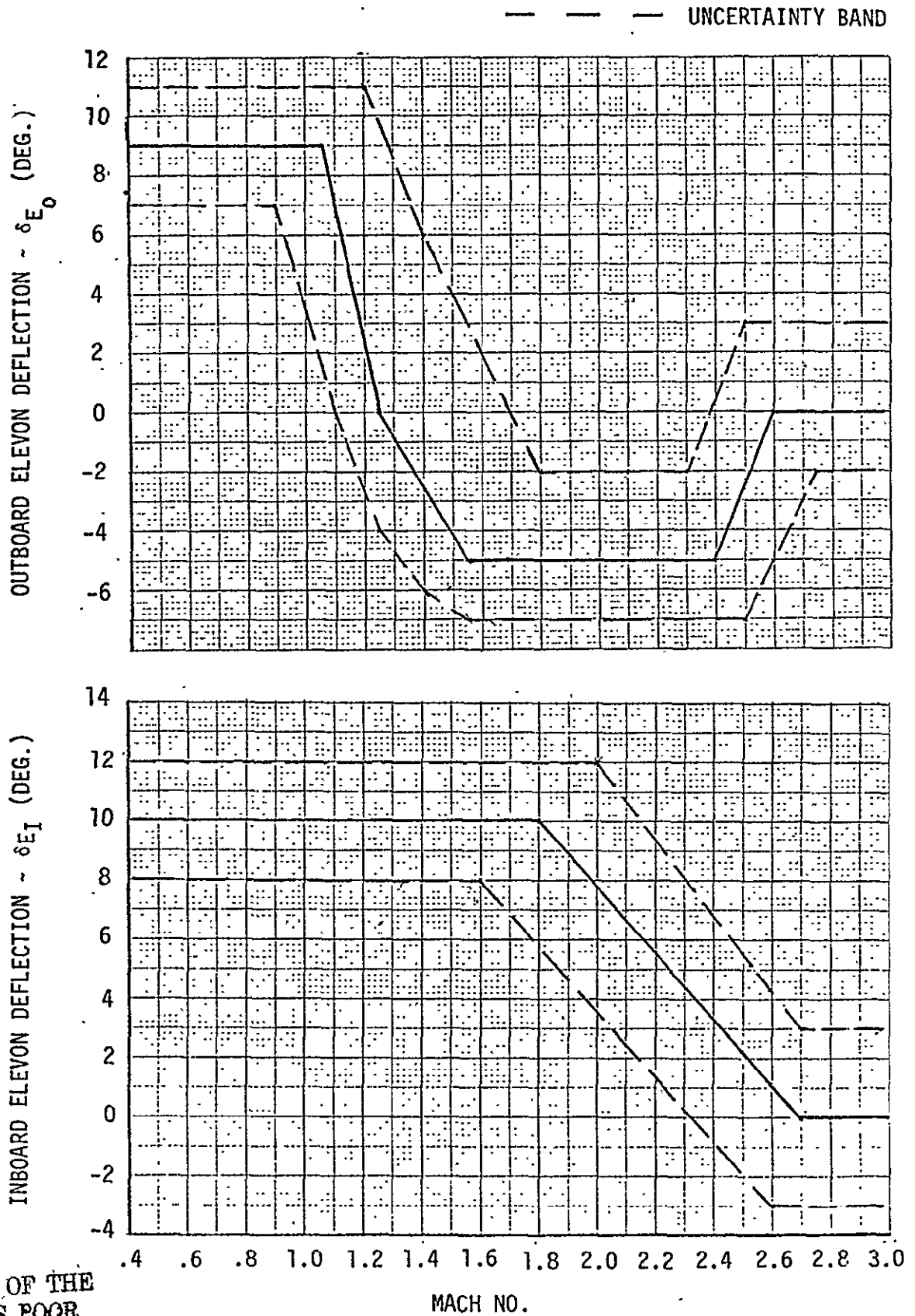
TEST CONDITIONS

The IA119 and the IA138 wind tunnel test program was essentially conducted in two parts. Part one was a power variation test at zero attitude, where chamber pressure of the MPS and SRB model nozzles was varied. Part two was a test program at a nominal power level that included various elevon deflections, nozzle gimbal patterns, and attitudes.

Base pressure data, from the power variation tests (Part 1), was evaluated at the test site along with prototype plume characteristics to evaluate the nominal model nozzle plume characteristics and model chamber pressures. (See Section V for plume simulation discussion). These tests were conducted at zero angle of attack and zero angle of sideslip. Tests were conducted for a series of Mach numbers from 0.6 to 2.5.

Part 2 of the test programs consisted of testing the model using the nominal power levels developed in Parts 1 over a range of attitudes and configurations (elevon deflections, gimbal angles, etc.). Data were obtained at nominal angles of attack of -8, -6, -4, 0, and +4 degrees.—The angles of sideslip were nominally 0, and ± 6 or ± 4 degrees.

Tests were conducted at various elevon deflections corresponding to Schedule 6 and probable variations about schedule 6. Schedule 6 elevon deflections are presented in Figure 3-1. Plots of the various inboard and outboard elevon deflection angles evaluated during the test along with the nominal schedule 6 value are presented in Figures 3-2 through 3-10. The elevon deflection closest to schedule 6 that was used to develop the plume induced aerodynamic data base is shown in each figure.



REPRODUCIBILITY OF THE ORIGINAL PAGE IS POOR

Figure 3-1. SCHEDULE 6 ELEVON DEFLECTIONS

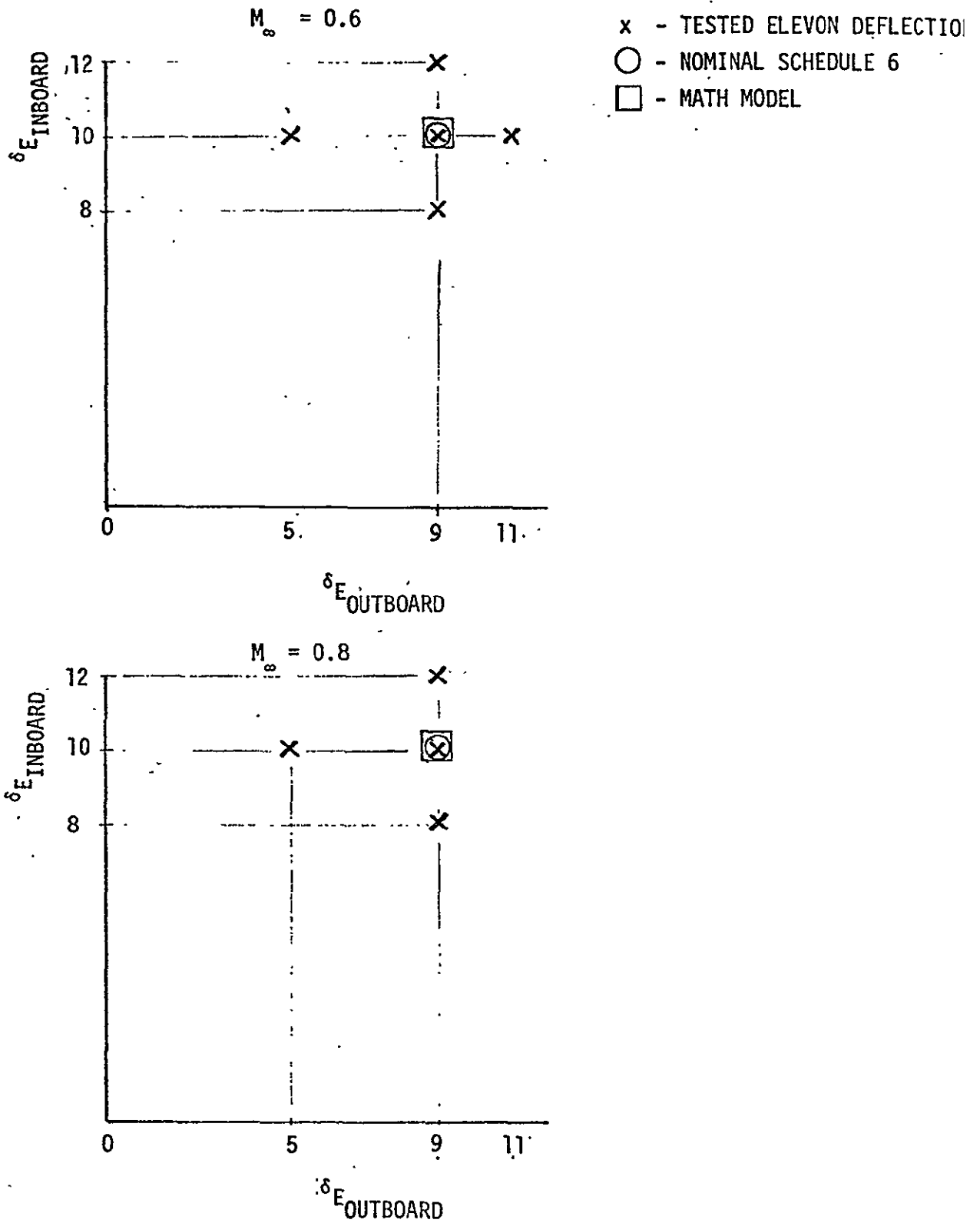


Figure 3-2. ELEVON SCHEDULE

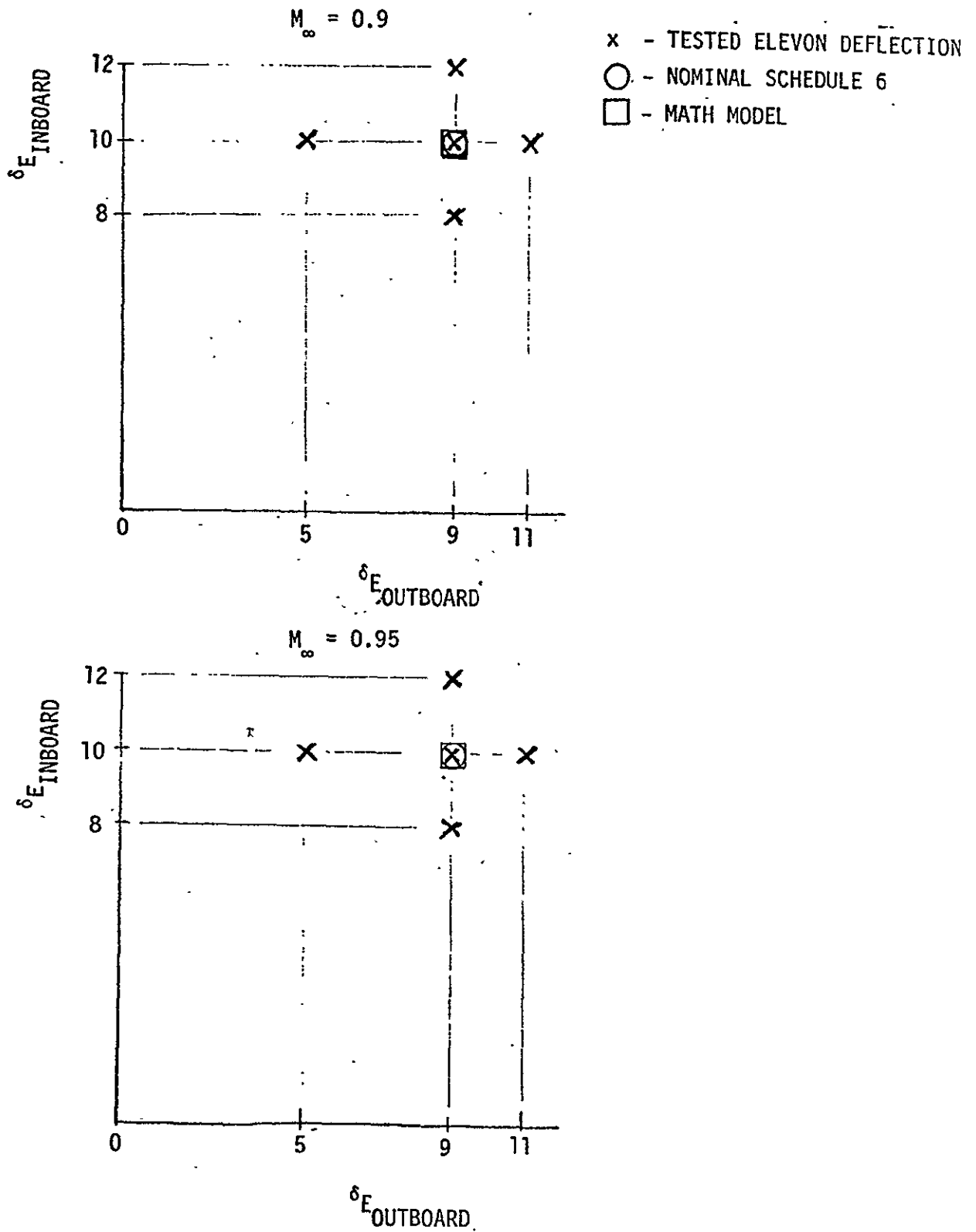


Figure 3-3. ELEVON SCHEDULE

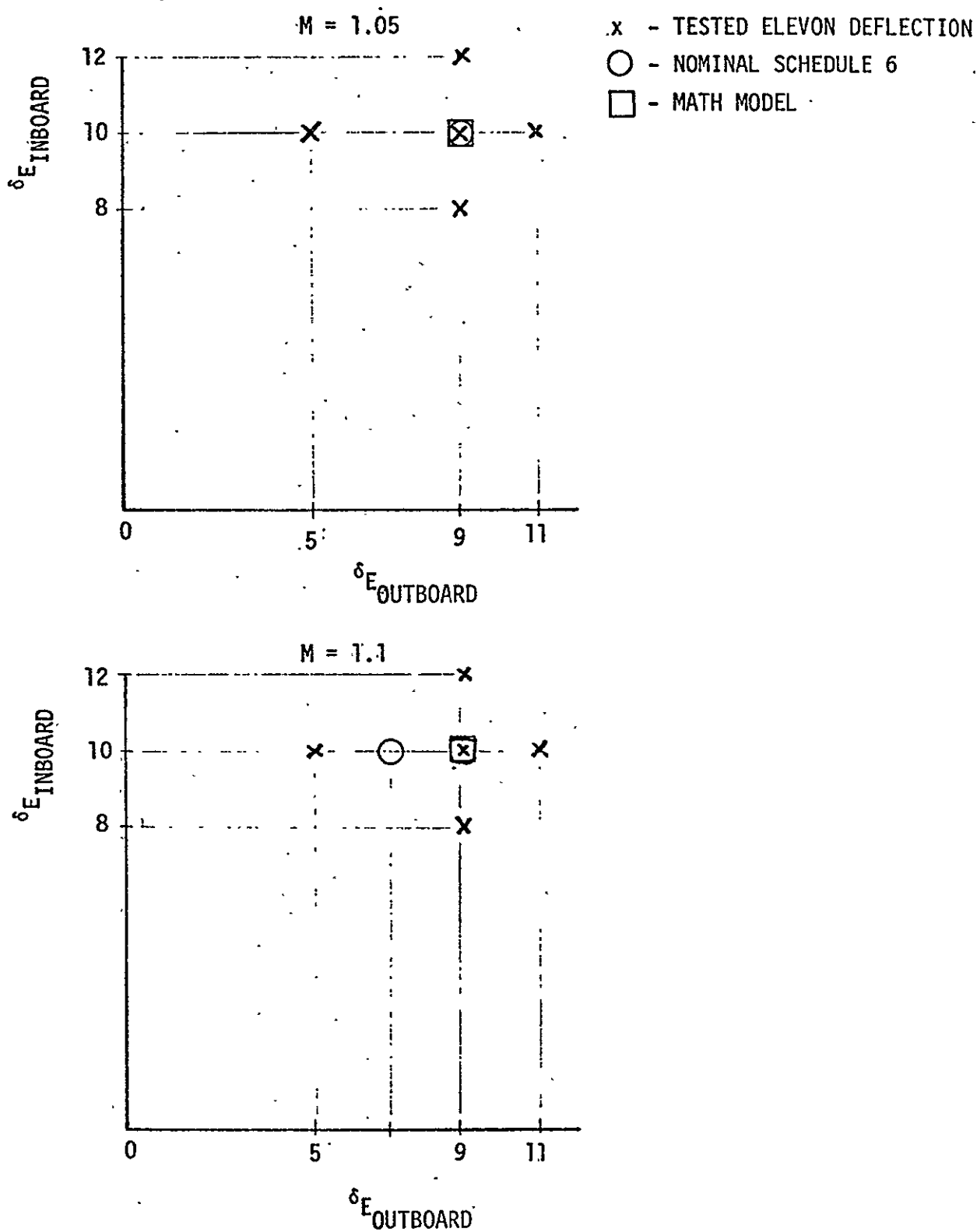


Figure 3-4. ELEVON SCHEDULE

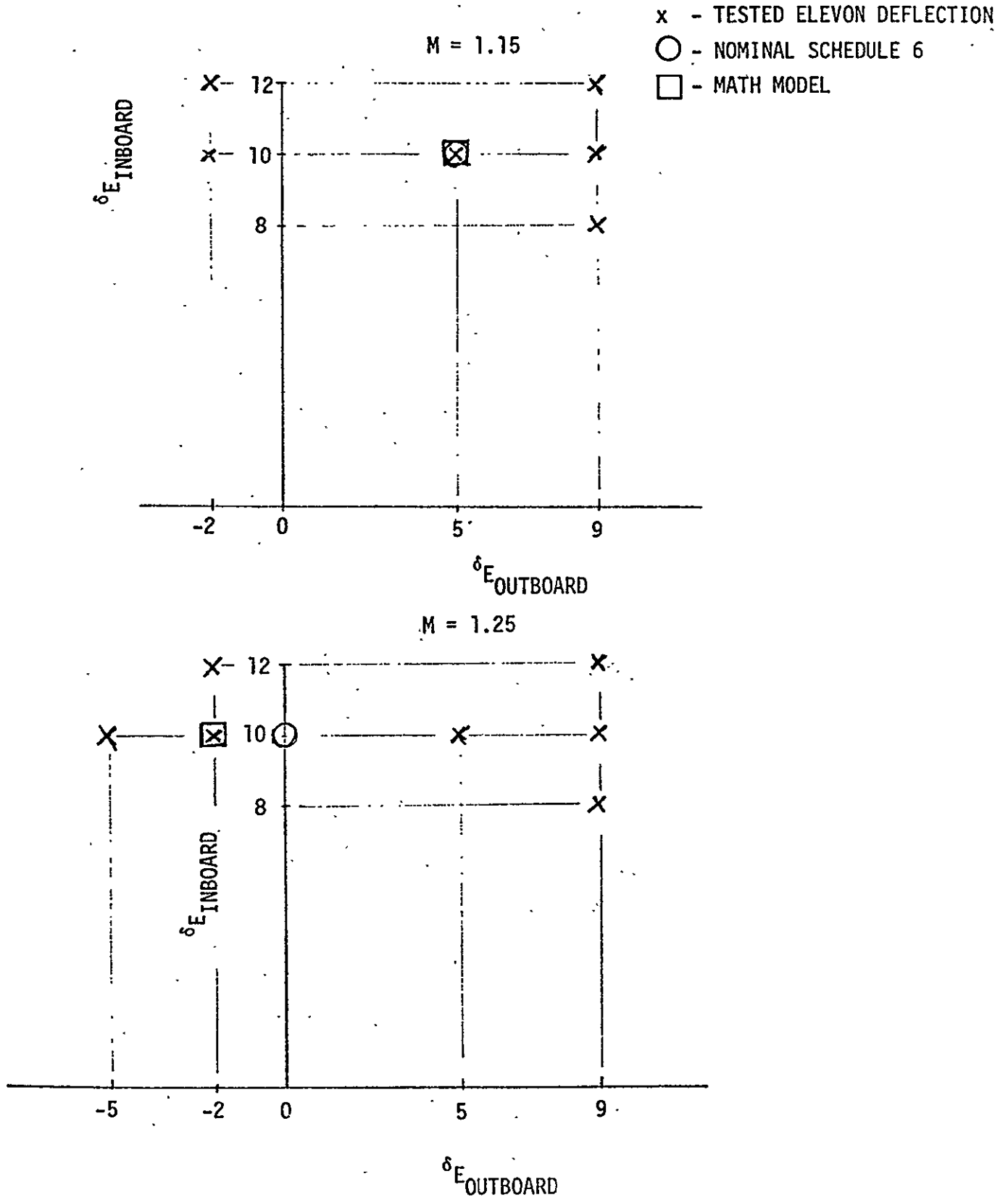


Figure 3-5. ELEVON SCHEDULE

- x - TESTED ELEVON DEFLECTION
- - NOMINAL SCHEDULE 6
- - MATH MODEL

$M_\infty = 1.4$

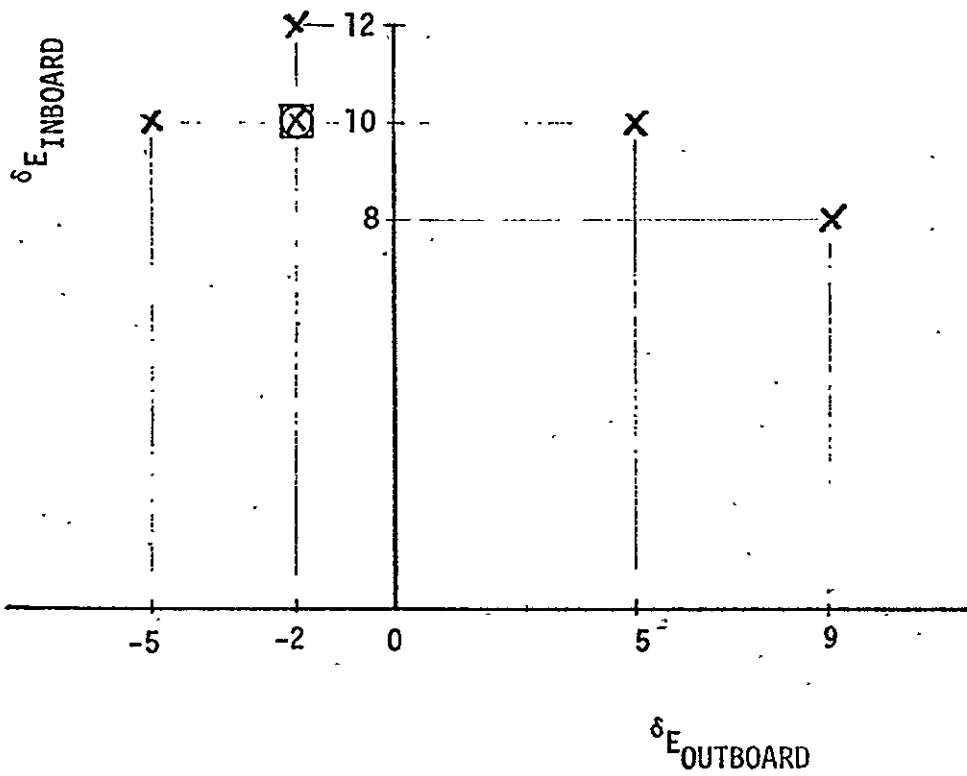


Figure 3-6. ELEVON SCHEDULE

- X - TESTED ELEVON DEFLECTION
- ⊙ - SCHEDULE 6
- ⊠ - MATH MODEL 10,-2

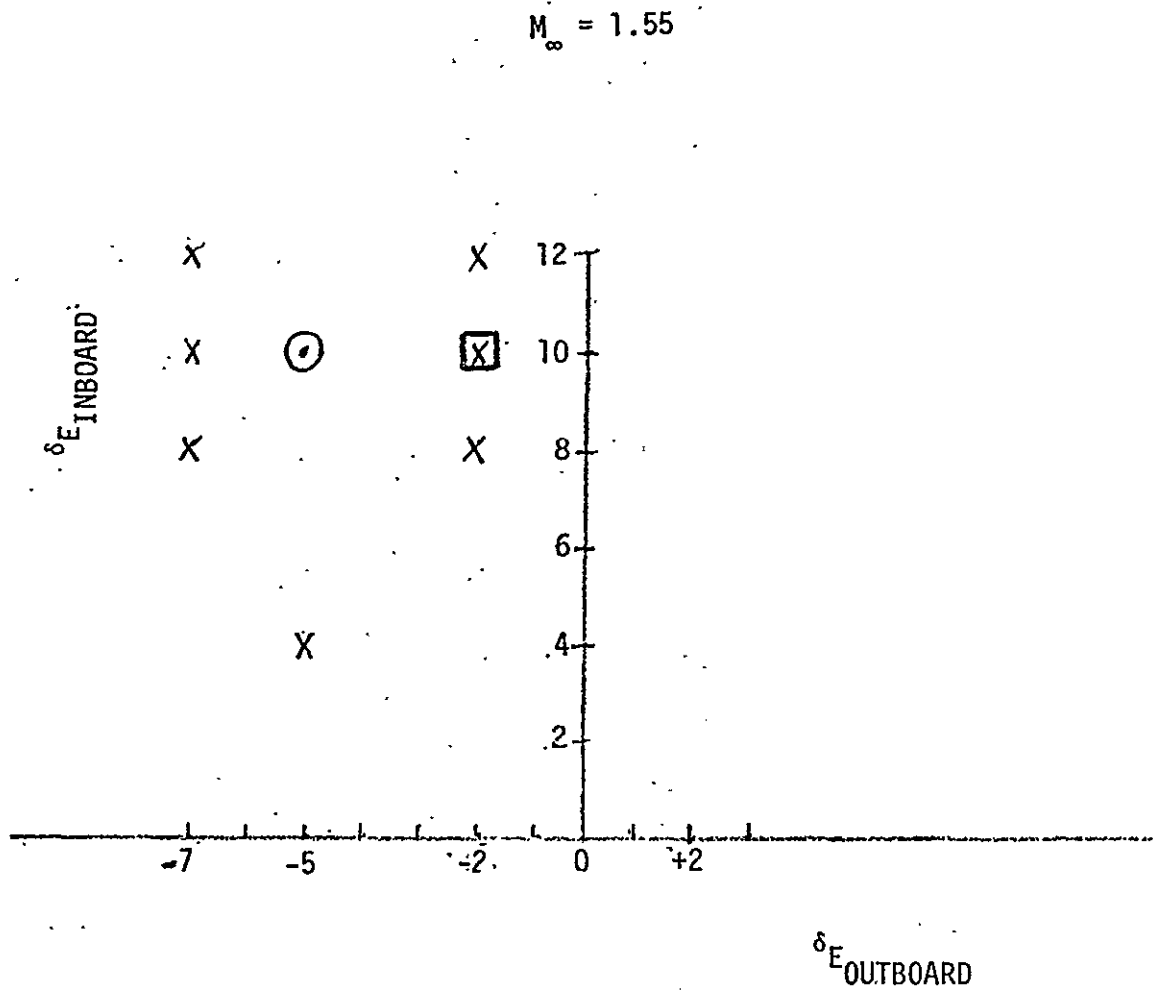


Figure 3-7. ELEVON DEFLECTION MATRIX ($M_\infty = 1.55$)

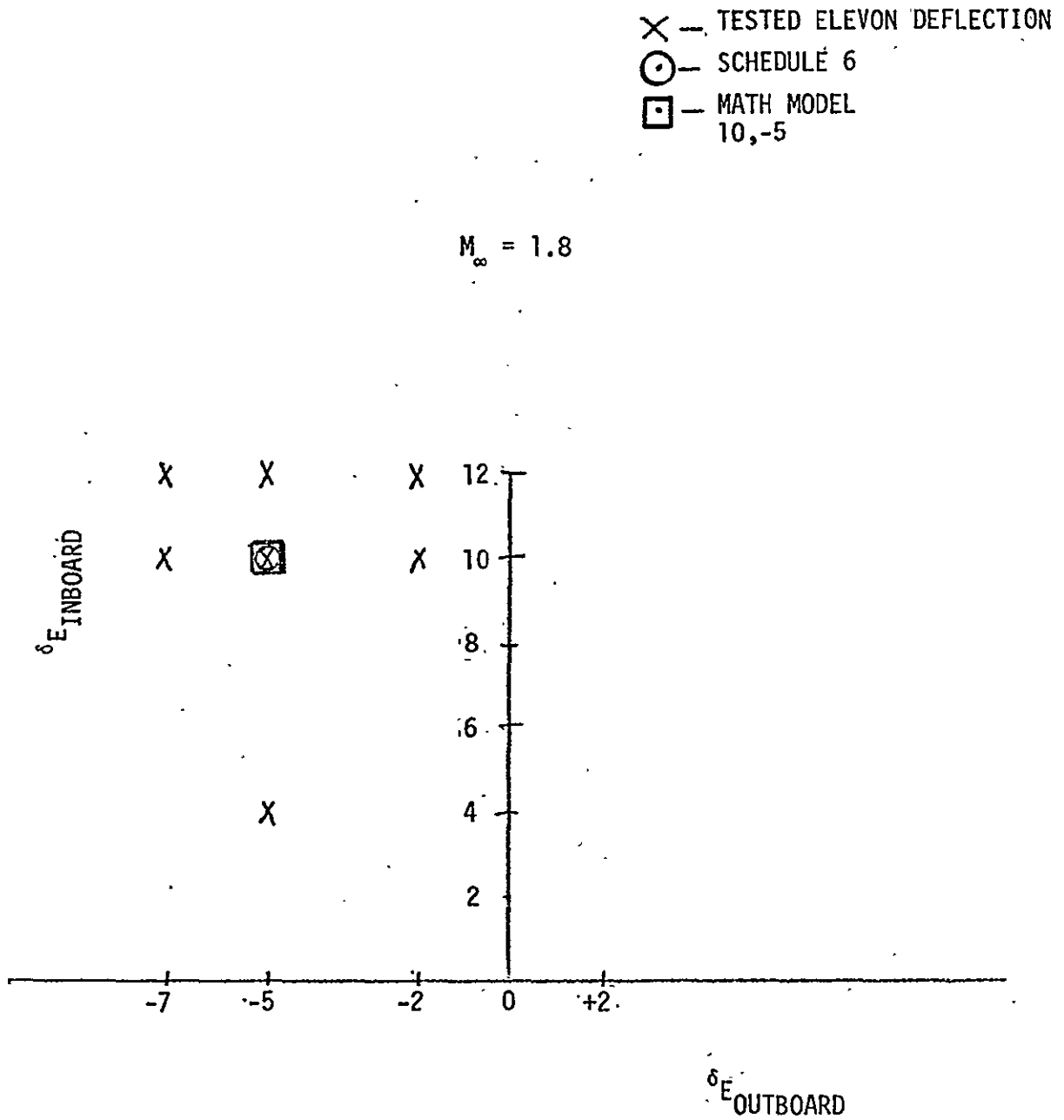


Figure 3-8. ELEVON DEFLECTION MATRIX ($M_\infty = 1.80$)

- ✕ — TESTED ELEVON DEFLECTION
- ⊙ — SCHEDULE 6
- ⊠ — MATH MODEL 4,-5

$M_{\infty} = 2.2$

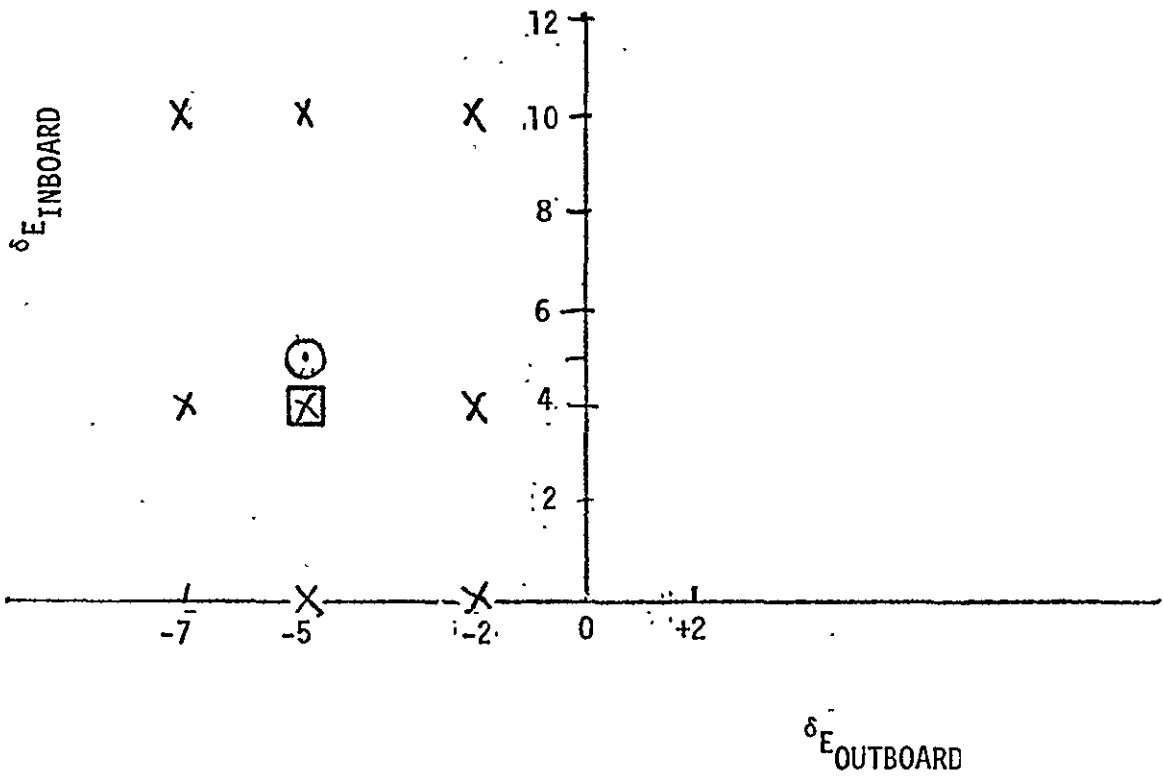


Figure 3-9. ELEVON DEFLECTION MATRIX ($M_{\infty} = 2.20$)

- × — TESTED ELEVON DEFLECTION
- ⊙ — SCHEDULE 6
- ⊠ — MATH MODEL 0,-2

$$M_{\infty} = 2.5$$

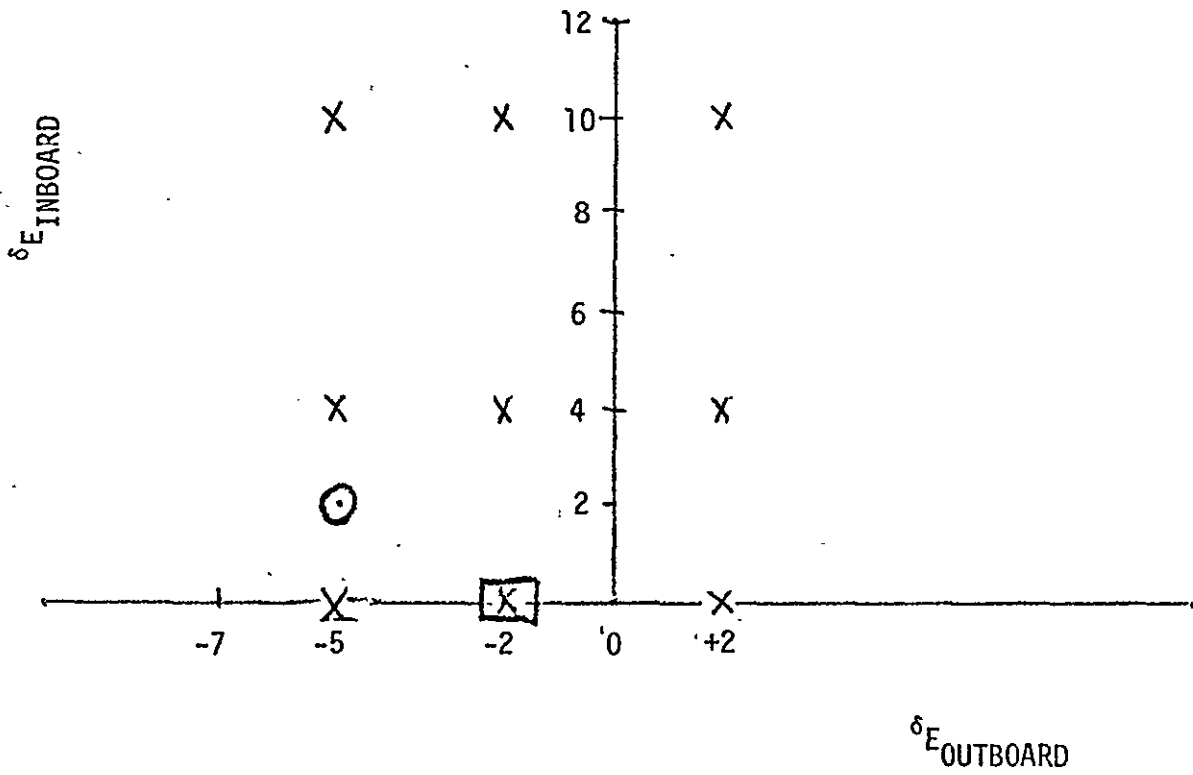


Figure 3-10. ELEVON DEFLECTION MATRIX ($M_{\infty} = 2.50$)

Section IV

WIND TUNNEL MODEL NOZZLE CALIBRATION ANALYSIS

An analysis of the model nozzle calibration data was performed to determine nozzle flow characteristics for the evaluation of model power levels. A range of model power levels were required for the power level variation portion of the test. Model nozzle wall pressures and exit plane pressures were plotted and compared with MOC results to evaluate the nozzle flow characteristics and to evaluate chamber to exit pressure ratios. The chamber to exit pressure ratios were required to evaluate the model plume characteristics.

Initially it was anticipated that several model nozzle configurations would be used during the IA119 test program and thus a considerable amount of calibration data were evaluated. The IA119 test program ultimately used only the 2% contoured SSME nozzle configuration and the 2% conical SRB nozzle configuration. The nozzle calibration tests were conducted for the IA19 Space Shuttle plume test (reference 5). This test (IA19) used essentially the same model hardware as the IA119 test. The IA138 test program used a 1% conical SSME nozzle configuration and a 1% conical SRB nozzle configuration.

Summary IA119 model nozzle performance data are presented in Figures 4-1 and 4-2 for the SSME model nozzles and the SRB model nozzles respectively. The average chamber to exit plane pressure used for the model SSME nozzle was 49.5. The average chamber to exit plane pressure used for the SRB nozzle was 66.0. These values were used to develop pretest pressure ratios for each Mach number.

Summary IA138 nozzle performance data are presented in Figures 4-3 and 4-4 for the SSME nozzles and the SRB nozzles respectively. The post-test SRB nozzle performance was slightly different from the pre test nozzle performance developed from the nozzle calibration data.

4-2

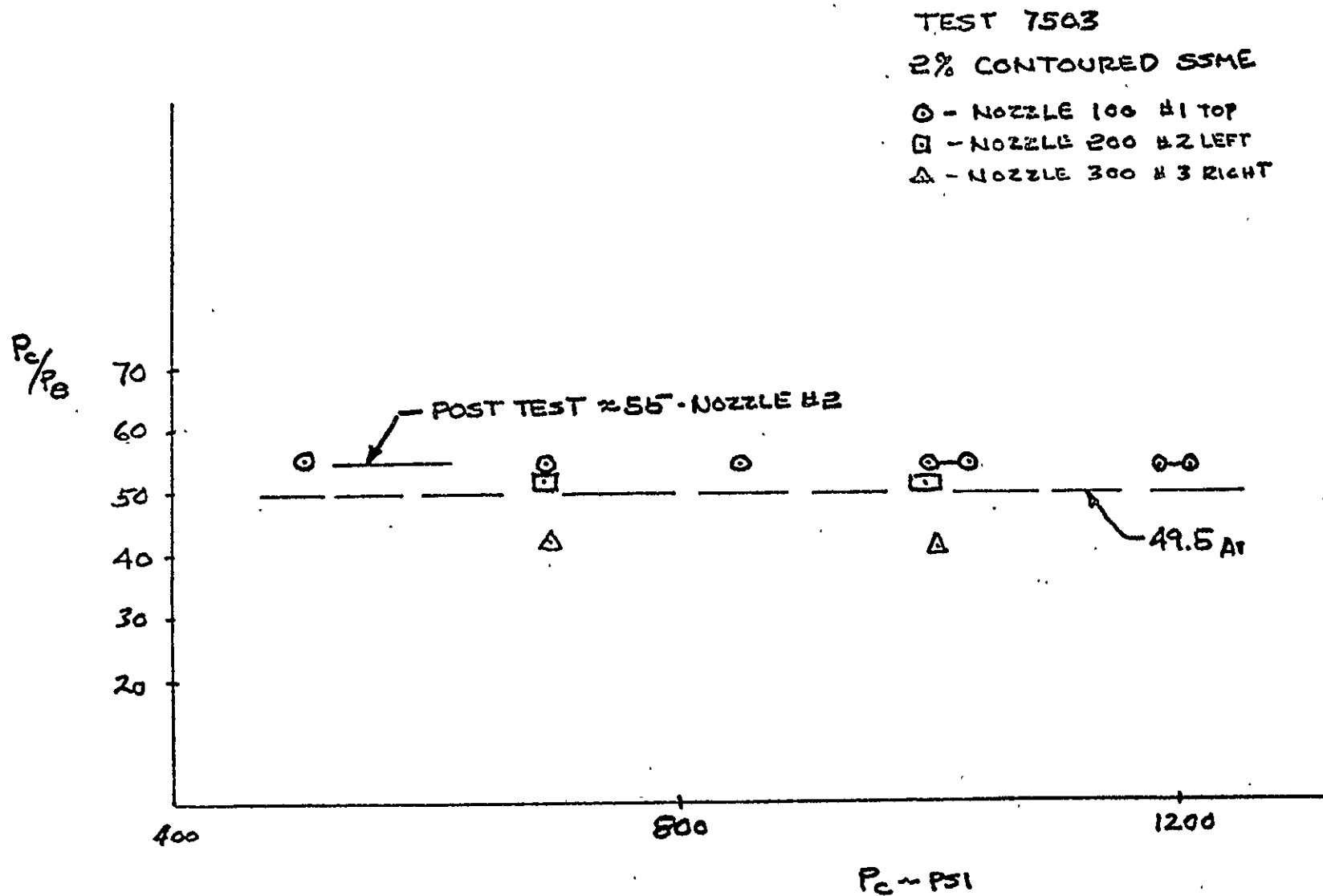


Figure 4-1. SSME NOZZLE CHAMBER TO EXIT PRESSURE RATIO - IA119

TR-1964

4-3

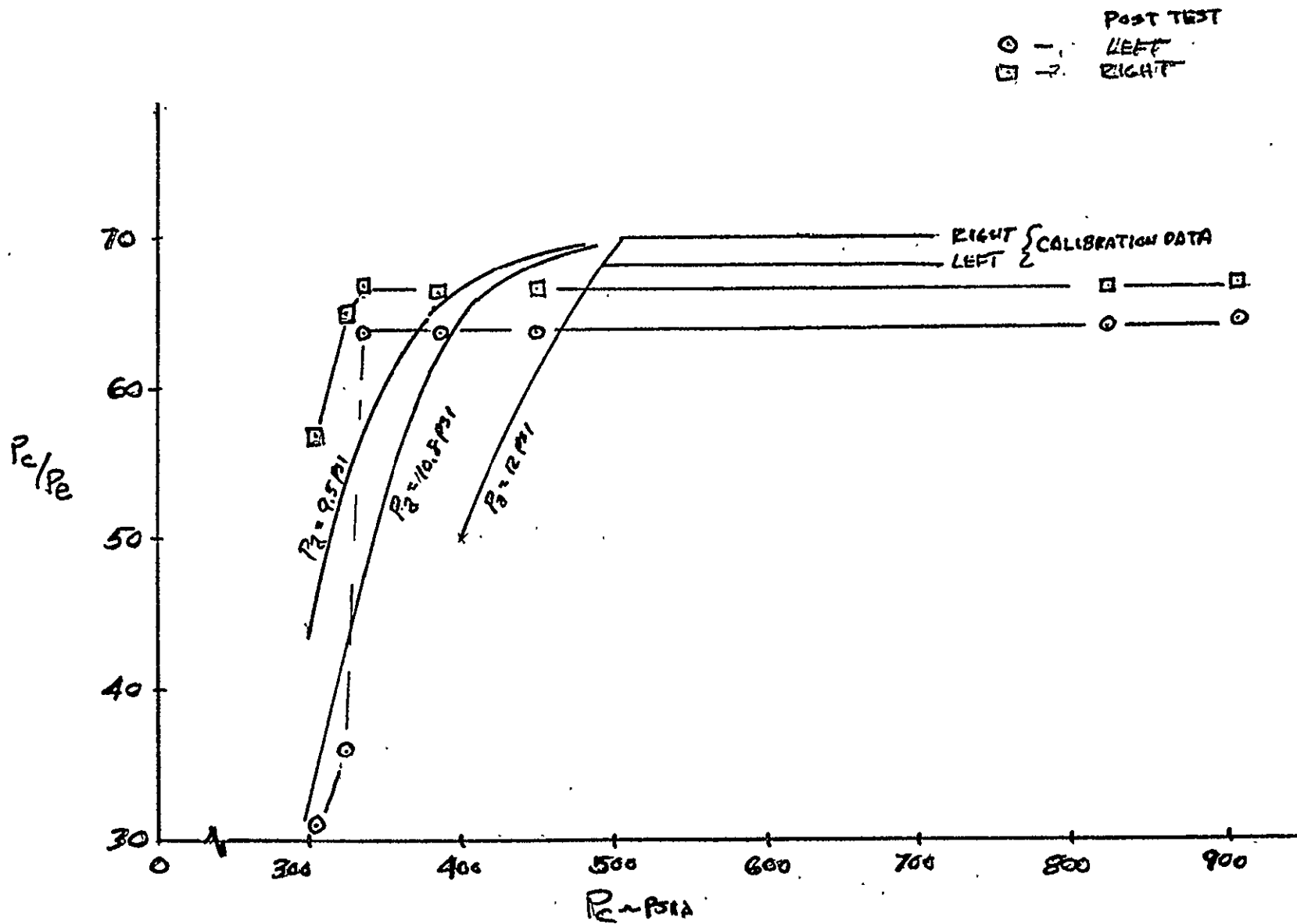


Figure 4-2. SRB NOZZLE CHAMBER TO EXIT PRESSURE RATIO - IA119

TR-1964

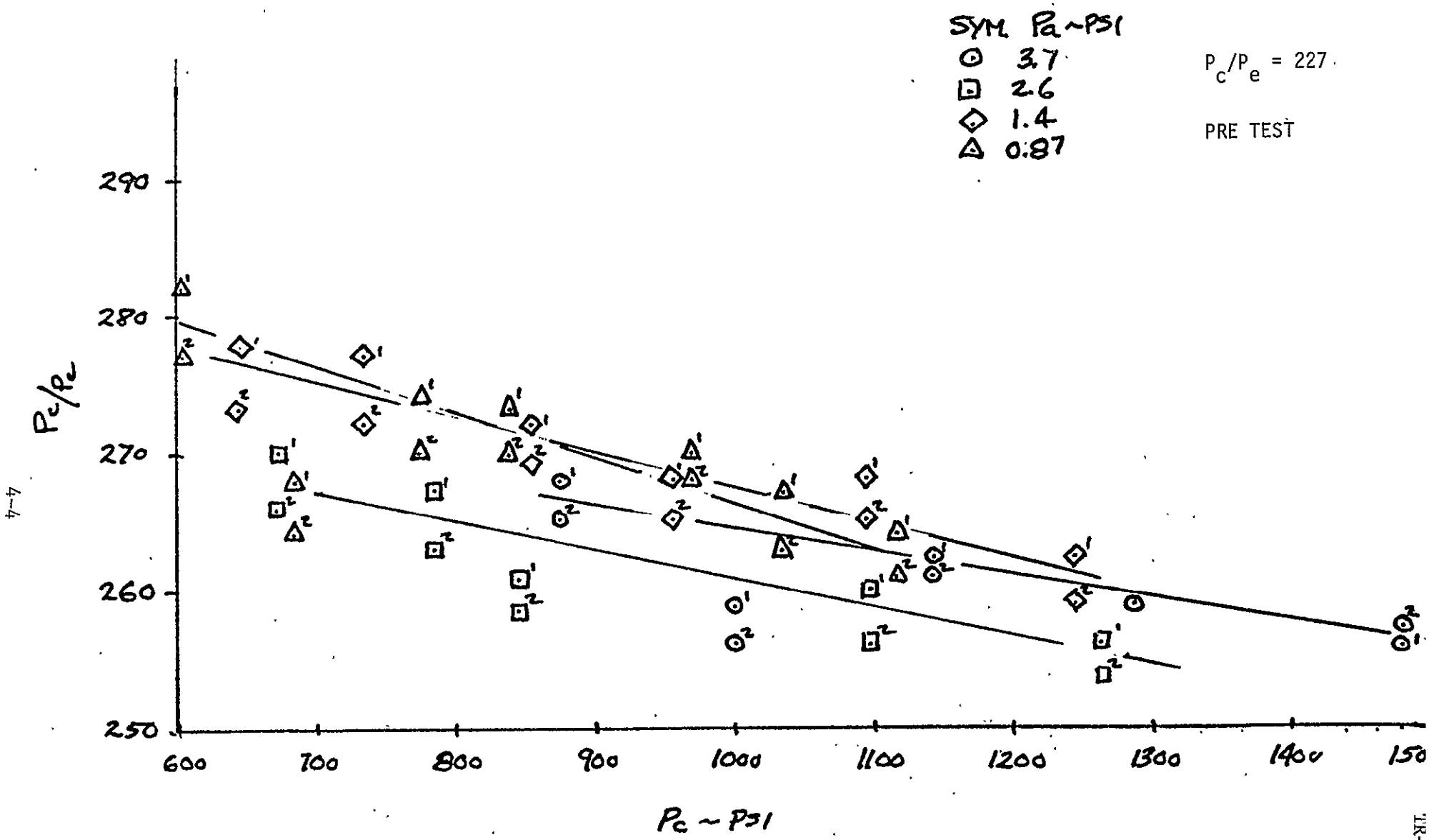


Figure 4-3. SSME NOZZLE CHAMBER TO EXIT PRESSURE RATIO - IA138

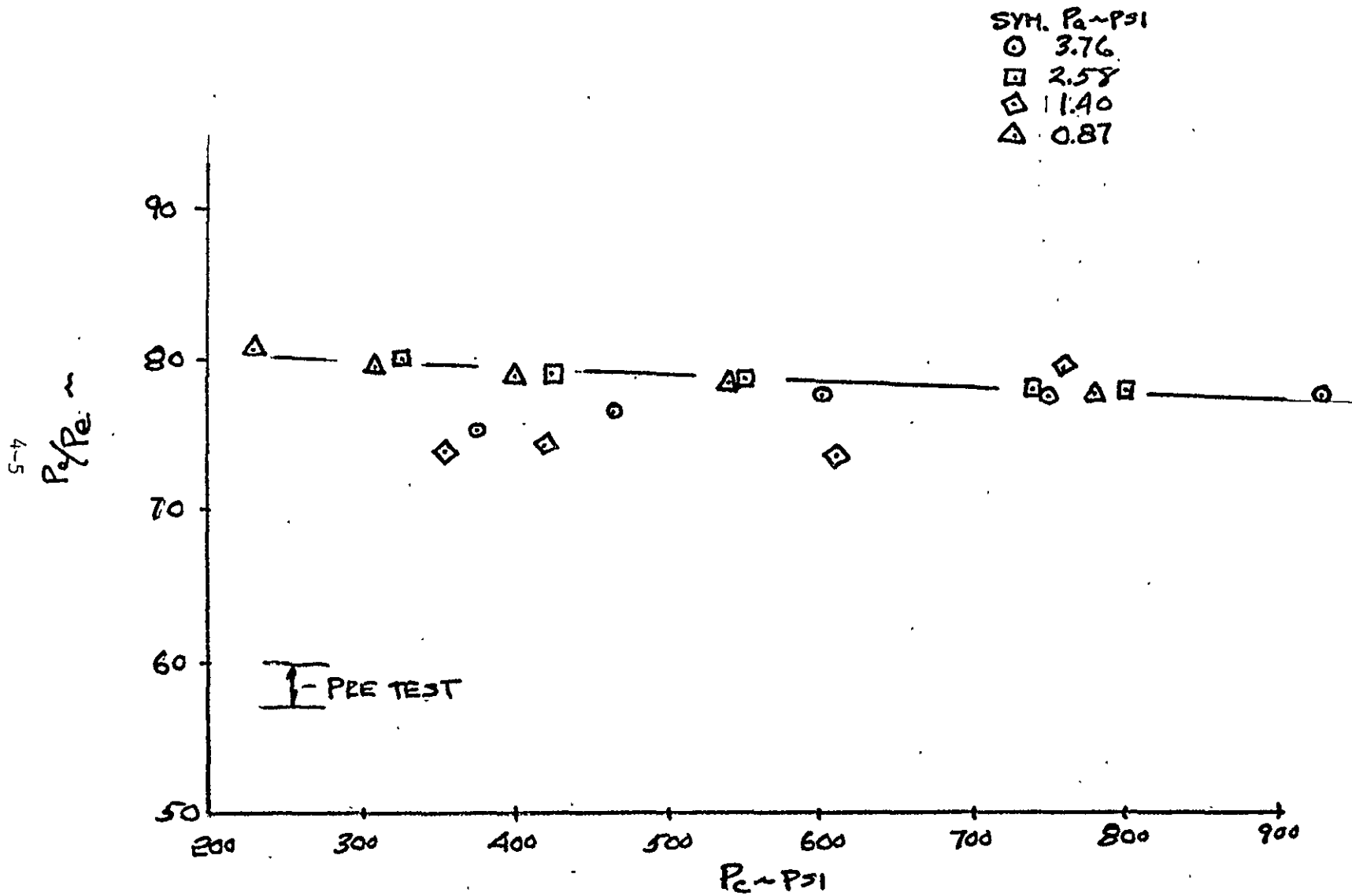


Figure 4-4. SRB NOZZLE CHAMBER TO EXIT PRESSURE RATIO — IA138

Section V

PLUME SIMULATION

The Space Shuttle plumes were simulated using cold air flowing through model nozzles. The model plume characteristics required to develop base and forebody pressure environments were determined using an iteration procedure requiring the development of "PROTOTYPE POSSIBILITY CURVES". Prototype possibility curves are curves of base pressure or base pressure coefficient versus prototype plume characteristics. An example prototype possibility curve is shown in Figure 5-1. The curve is called possibility curve since it is developed for a range of possible prototype base pressure environments. These curves were developed prior to the wind tunnel test for both the SSME and SRB prototype nozzles. The SSME possibility curves were developed using possible orbiter base pressure coefficients and the SRB possibility curves were developed using SRB possible base pressure environments. During the power level portion of the test, model base pressure data are plotted on the prototype possibility curves as shown in Figure 5-1. The model power level is determined where the model pressure curve crosses the prototype pressure curve. An iteration procedure is used when there are two variables involved that influence the base pressure, i.e. SSME power level and SRB power level. The possibility curves and the model pressure data used to determine the nominal power levels at each Mach number are presented in the Appendix of references 1 and 2.

The form of the plume simulation equation used during the IA119 and IA138 test program was the following (reference 6)

$$\delta_j \gamma_j^N \text{ PROT.} = \delta_j \gamma_j^N \text{ MODEL}$$

where N is a function of Mach number. A plot of N versus Mach number is shown in Figure 5-2 and was obtained from reference 7. This curve was developed by correlating the base pressure in the near field and the far field developed from cold gas air and CF_4 plumes. The plume induced near field and far field areas considered are shown in Figure 5-3. The model configurations used were single body single nozzle, single body triple nozzle and triple body configurations. The triple body configuration was similar to the ET-SRB space shuttle

configuration. The band on the curve represents the range of N for the various models used in the plume technology test (i.e., single body, triple body, etc.). The criteria used for correlation of the plume technology data was that the same base pressure occur for a five percent or less change in similarity parameter. The band represents the total spread of N for the various model and nozzle configurations considered in the plume technology program.

Recent analysis (Reference 8) has identified a new similarity parameter that has the functional form

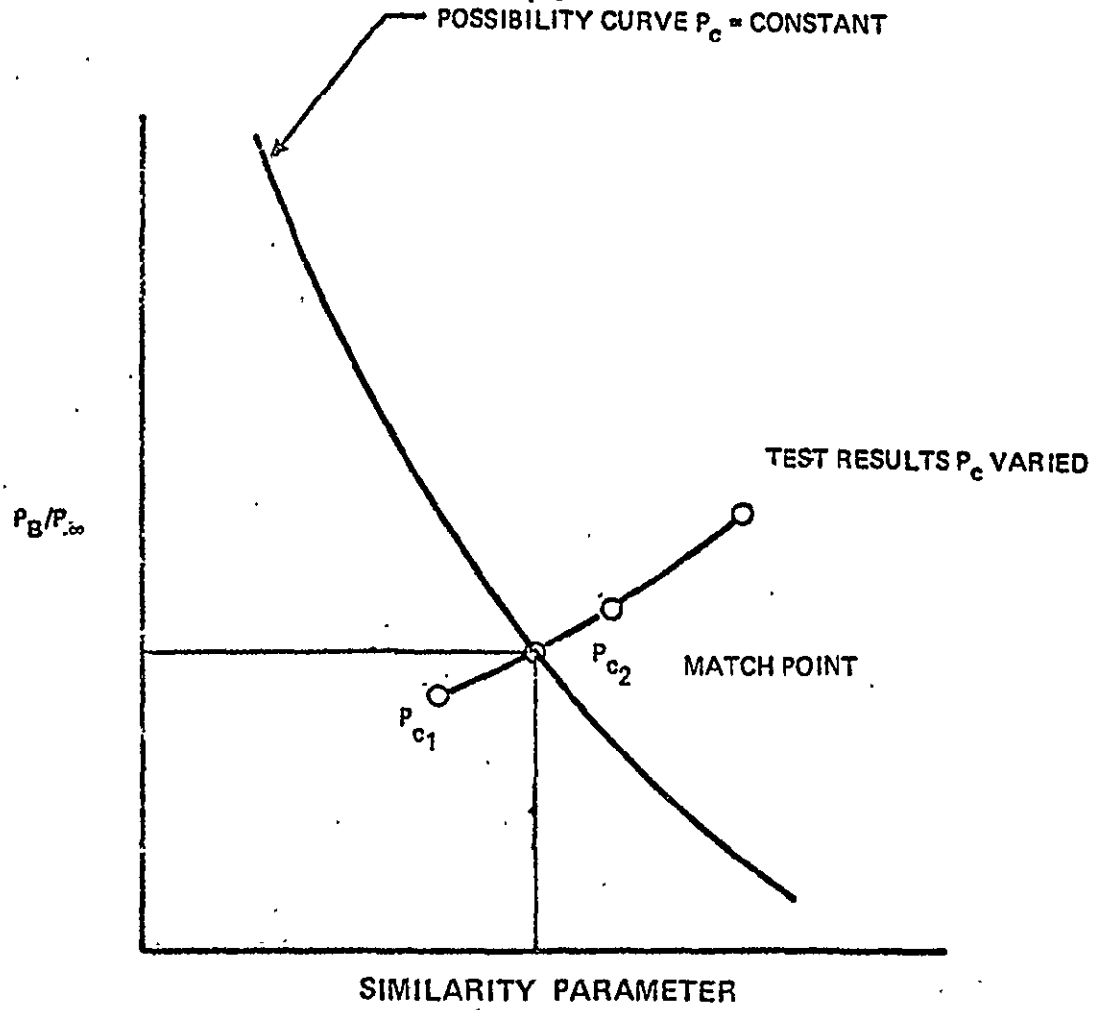
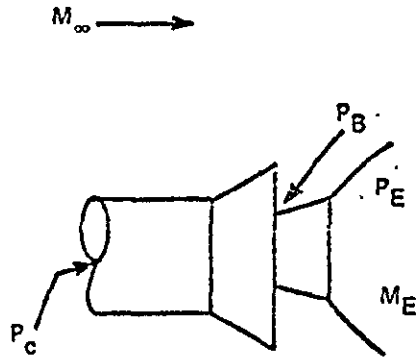
$$\frac{M_j \delta_j}{f(M_{EX}) g(\gamma_j)}$$

where f, g appear to depend weakly upon M_∞ and configuration.

The functions f and g have been defined for several model configurations and Mach numbers. The form of the various base pressure correlation parameters is presented in Table 5-1. These new similarity parameters, namely

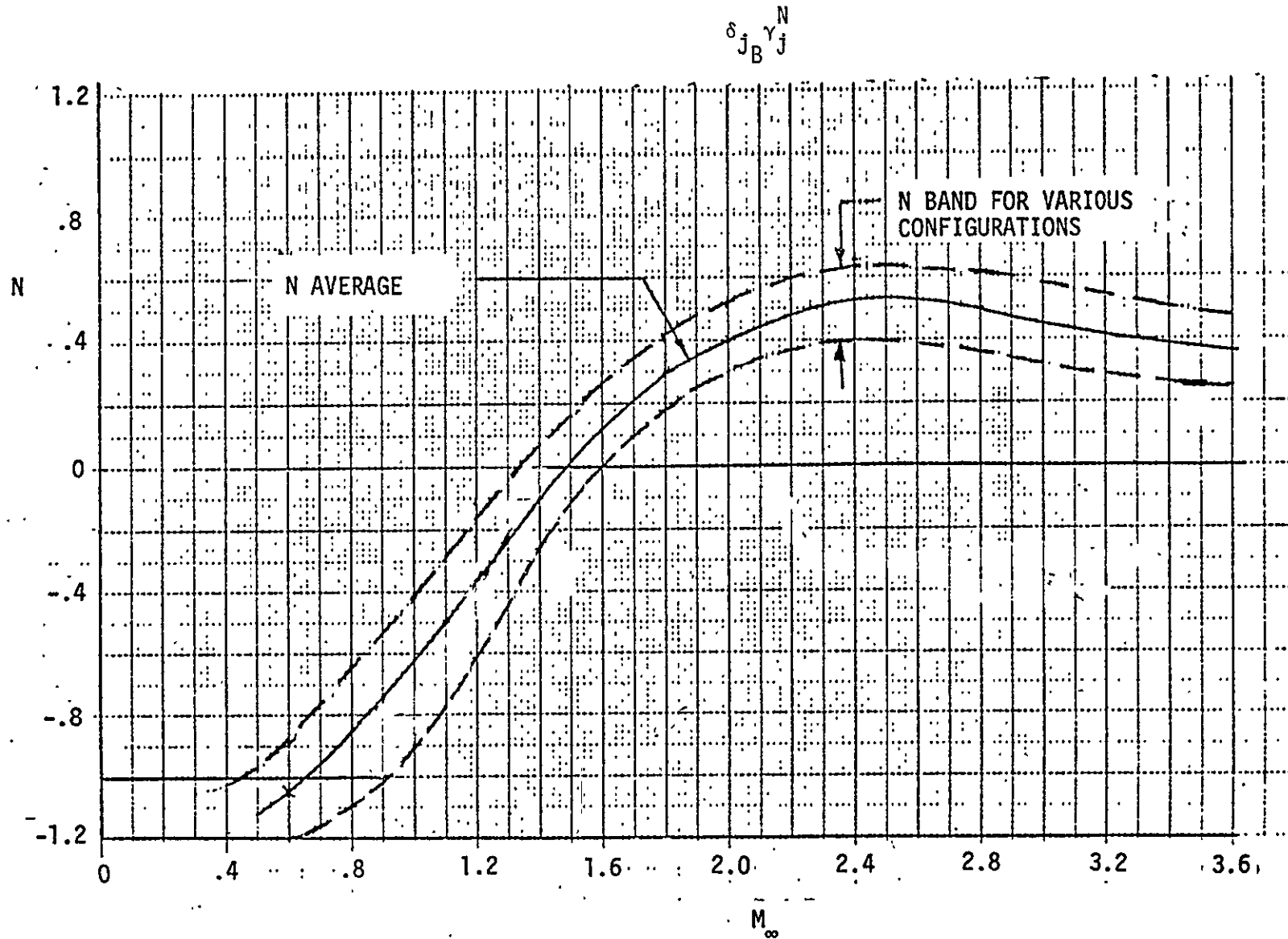
$$\frac{M_j \delta_j}{M_E (.25) \gamma_j}, \quad \frac{M_j \delta_j}{M_E (.25) \gamma_j (.5)}, \quad \text{and} \quad \frac{M_j \delta_j}{\gamma_j}$$

for the IA138 test results along with the value of $\delta_j \gamma_j^N$ (see Section VII).



5-3

Figure 5-1. PROTOTYPE POSSIBILITY CURVE



5-4

Figure 5-2. SIMILARITY PARAMETER EXPONENT

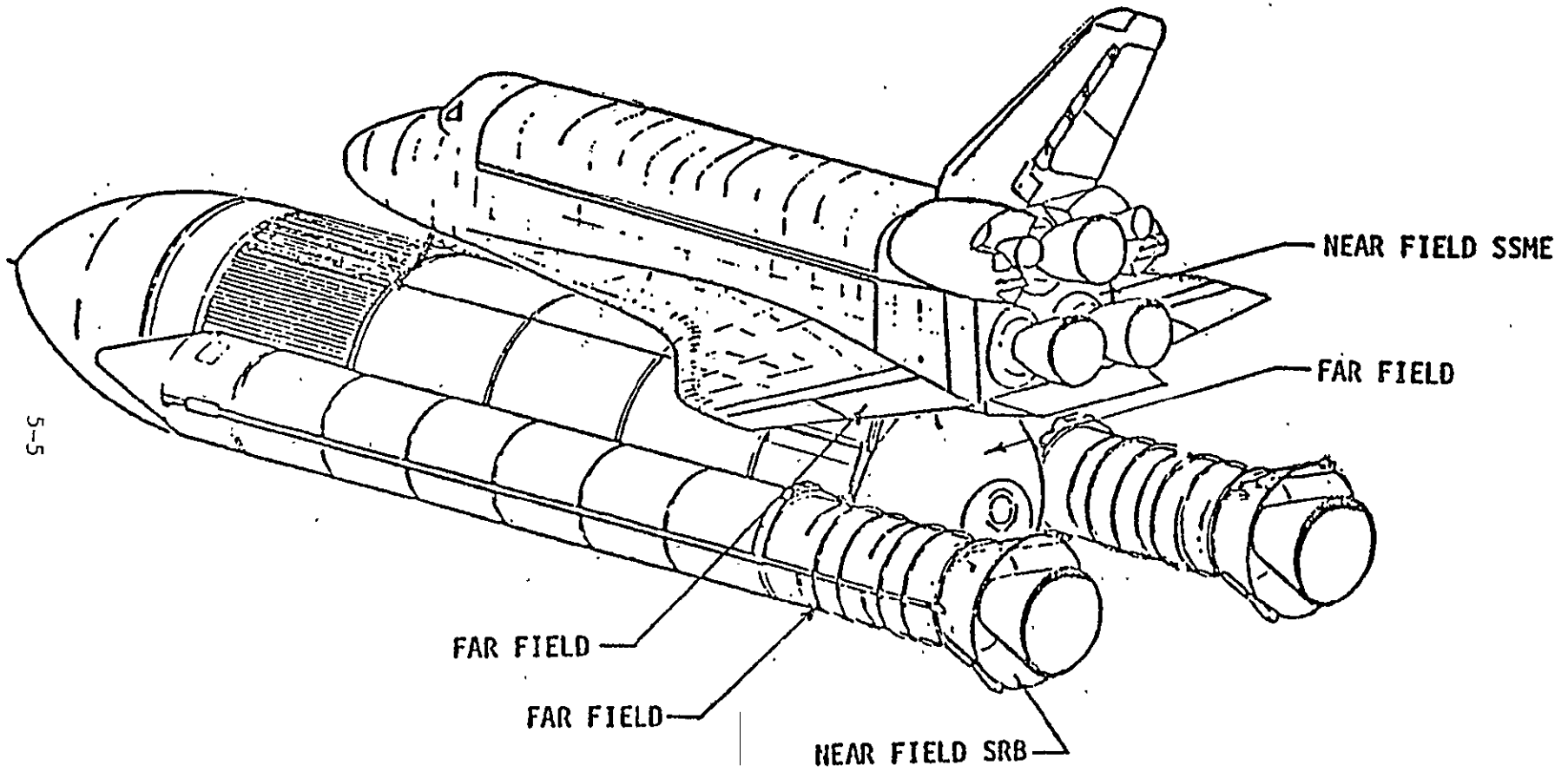


Figure 5-3. PLUME FLOW FIELD AREAS

Table 5-1
CORRELATION PARAMETERS

M_0	CONFIGURATION		
	SINGLE BODY SINGLE NOZZLE	SINGLE BODY TRIPLE NOZZLE	TRIPLE BODY
0.9	$\frac{M_{j\delta j}}{M_{EX}^{0.25} \gamma_j}$	$\frac{M_{j\delta j}}{M_{EX}^{0.25} \gamma_j}$	$\frac{M_{j\delta j}}{M_{EX}^{0.25} \gamma_j}$
1.2	$\frac{M_{j\delta j}}{M_{EX}^{0.25} \gamma_j^{0.5}}$	$\frac{M_{j\delta j}}{M_{EX}^{0.25} \gamma_j}$	$\frac{M_{j\delta j}}{M_{EX}^{0.25} \gamma_j}$
1.46	$\frac{M_{j\delta j}}{M_{EX}^{0.25} \gamma_j^{0.5}}$	$\frac{M_{j\delta j}}{M_{EX}^{0.25} \gamma_j}$	
3.48	$\frac{M_{j\delta j}}{\gamma_j}$	$\frac{M_{j\delta j}}{\gamma_j}$	

Section VI
DATA ANALYSIS

Five computer codes were used to analyze the test data. These programs are: 1. SORT program, 2. Power Delta program, 3. Sigma V Punch, 4. Wind Tunnel Pressure Data Analysis and 5. Plume Integration. A brief discussion of each of these programs is presented below.

SORT PROGRAM

The SORT Program was used to sort the run and sequence data sets into basic groups of four. The four run groups consist of $+\beta$ power-on, $+\beta$ power-off, $-\beta$ power-on and $-\beta$ power-off. The four run data sets were arranged in angle of attack sets of $-8, -4, 0, 4$. Flags were set to note α, β , Mach, gimbal and configuration incompatibility of the four run sets.

The following tolerances were put on the data sets to check compatibility.

VARIABLE	TOLERANCE
MACH	.03
α	.25
β	.25
β	Sign
Gimbal	$\neq 0$
CONFIGURATION NO. DO NOT AGREE	
RUN NUMBER/SEQUENCE OUT OF PLACE	
δ_{INB}	$\pm .25$
δ_{OUT}	$\pm .25$

The SORT program proved very useful in identifying errors in the post test run schedule and differences between the power-on and power-off model attitude.

POWER DELTA PROGRAM

The Power Delta program was used to evaluate the change in the pressure data due to power. The program lists all data from the power on run and all data from the power off run and then subtracts the two data sets and lists the power delta's. This allows a rapid survey of the power delta's for abnormal numbers and a reference to the power on run and power off run to determine the error source.

SIGMA V PUNCH

The Sigma V Punch program was used in conjunction with the Power Delta program to sort the forebody power delta data into various elements and components and punch cards of the power delta in a format compatible with the "Wind Tunnel Pressure Data Analysis Program - WTPDA". WTPDA is an interactive graphic pressure data integration computer program which operates on the Sigma V Graphics System.

WIND TUNNEL PRESSURE DATA ANALYSIS (WTPDA)

WTPDA is an interactive computer graphics program which allows an engineer to apply his judgement to the smoothing of wind tunnel pressure data in a real time environment. The purpose of the program is to produce airloads which are compatible with vehicle stability data and which reflect engineering judgement. WTPDA employs interactive computer techniques so that an engineer can develop balanced airloads in a timely manner.

WTPDA can integrate pressure data on wings, vertical stabilizers, fins, cylinders, and arbitrary cross-section fuselages. Although WTPDA was developed specifically to handle the Space Shuttle launch vehicle, it is capable of handling almost any arbitrary cross-section body.

The WTPDA program was used to plot and smooth the power delta CP's on the forebody. Only limited integration of pressures were performed to check the main pressure integration computer program which is discussed below.

PLUME INDUCED PRESSURE INTEGRATION

The Plume Integration computer program was the main tool used to analyze the IA119 and IA135 pressure data. This computer program was developed

specifically to analyze the IA119 pressure data and was used to integrate the pressure data to obtain base and forebody plume induced aerodynamic loads and moments. The computer program was developed to analyze four run sequences of positive and negative β sets. This operation is required since portions of the model have pressure data on only one side. Thus, to analyze the effects of sideslip required the evaluation of + and - β runs. Both power-on and power-off data sets are required since a portion of the plume induced data uses power on pressure coefficients while other portions require only the change in pressure coefficient due to power.

The analysis of the plume induced aerodynamic characteristics was performed using different pressure data over different portions of the vehicle. This type of analysis was required because of the unique configuration of the Space Shuttle and the model configurations used to obtain the forebody aerodynamic characteristics. The two types of pressure data used for analysis are: 1) The power on C_p 's for nominal SSME and SRB model power settings; and 2) The power delta C_p 's where $\Delta C_{p_{Power}} = C_{p_{Power\ on}} - C_{p_{Power\ off}}$.

The power on C_p 's were used to evaluate the power-on base forces and moments. The power delta C_p 's were used to evaluate the change-in forebody aerodynamic characteristics. The location on the Space Shuttle vehicle where the different types of pressure data were used is shown in Figure 6-1. The results of integration of the base pressure and the forebody power delta pressures have been listed in a special format which is discussed in Section VII.

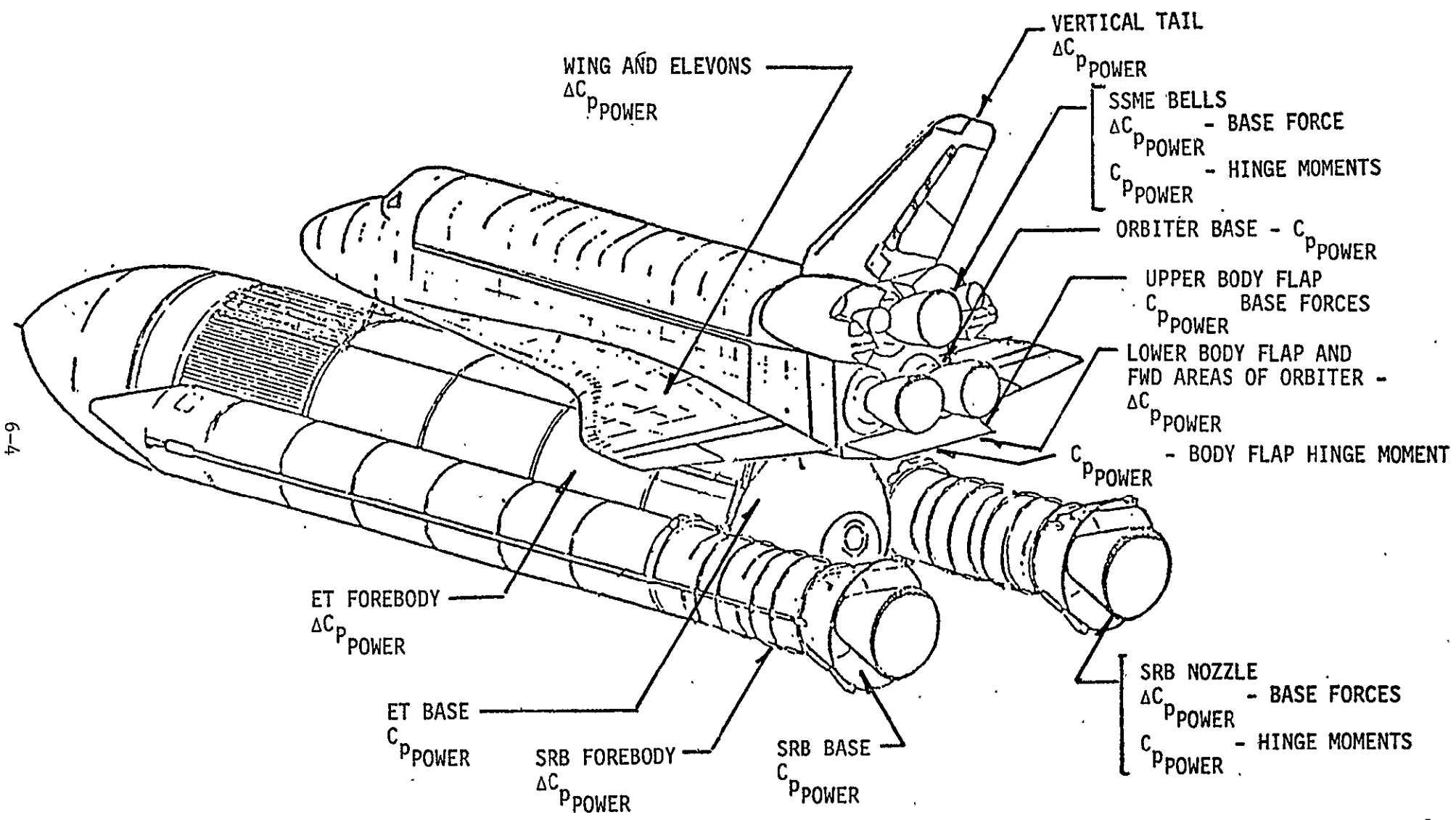


Figure 6-1. PLUME FLOW FIELD AREAS

Section VII
TEST RESULTS

The results of the integration of the base pressure and forebody power delta's are presented in table form in the Appendix of references 1 and 2. The output of the Plume Integration computer program contains all the results of the pressure integration including base coefficients, forces and moments and forebody coefficient data from pressure integration along with the gage data.

An example of the printout of a data set from test IA119 is presented below. The data are arranged in 9 sections. Section 1 presents the run numbers, Mach number, vehicle configuration, and attitude. Section 2 presents the nozzle gas dynamic properties. Section 3 presents the nozzle gas dynamic similarity parameter. Section 4 presents the results of the pressure integration over the base elements and components. Section 5 presents the average base pressure coefficient for each element. Section 6 presents the nozzle average base pressure coefficients. Section 7 presents the nozzle hinge moment data. Section 8 presents the forebody data from the gages. Section 9 presents the forebody data from pressure integration.

IA119 TEST DATA FORMAT

REPRODUCIBILITY OF THE ORIGINAL PAGE IS POOR

Table with 9 numbered sections containing test data for IA119. Section 1: Run sequence code 20501, Mach 3.499, Alpha -7.91, Beta -1.0. Section 2: Nozzle conditions including throat area, exit area, and pressure ratios. Section 3: Similarity parameters like Mach number and nozzle length. Section 4: Base pressure coefficients for various elements. Section 5: Average base pressure coefficients. Section 6: Nozzle average base pressure coefficients. Section 7: Nozzle hinge moment data. Section 8: Forebody data from gages including vertical tail and right wing. Section 9: Forebody data from pressure integration.

Printouts of each run sequence set is presented in the Appendix of reference 1. The data sets are grouped for a constant Mach number. The first data set within a Mach group is the power-off runs. The second group contains the variable power runs. The third group are the various elevon deflections. The fourth group contains the various gimbal angle runs and the fifth group is a 90° roll run sets.

An example of the printout of a data set from test IA138 is presented below. The data are arranged in 9 sections. Section 1 presents the run numbers, Mach number, vehicle configuration and attitude. Section 2 presents the nozzle gas dynamic properties. Section 3 presents the plume gas dynamic similarity parameters. Section 4 presents the values of parameters used to determine the similarity parameters. Section 5 presents the results of the pressure integration over the base of the elements and components. Section 6 presents the average base pressure coefficient for each element. Section 7 presents the nozzle average base pressure coefficients. Section 8 presents the forebody data from the gages. Section 9 presents the forebody data from pressure integration.

IA138 TEST DATA FORMAT

REPRODUCIBILITY OF THE ORIGINAL PAGE IS POOR

①	②	③	④
1 RUN SEQUENCE--2201--7700 MACH 1.300 ALPHA -.120 BETA -.110 ATTITUDE ALPHA=0 BETA=0 CONFIGURATION 1 EL1410.00 EL07-2400 NOZZLE GIMBAL .00 TUNNEL TOTAL 550.70	2 NOZZLE CONDITIONS SSSE PCZ 670.26 PCAN 350.16 PCZ 670.10 PIST 304.00 APZ 2.51 PZC 0.30 PCP 100.00 PZC 3.60 PCPE 378.05 PCPE 74.90 PCZPC 268.47 PCSPZ 79.90 DELJ 16.56 DELJ 37.30 DELJ 2 16.71 DELJ 3 36.03 DELJ 4 24.01 DELJ 5 24.20 CPZ 2 11.00 CPZ 3 11.00 CPZ 4 11.00 CPZ 5 11.00	3 SIMILARITY PARAMETER 11 DELJANNAJ NOZZLE 1 X 20.22 NOZZLE 2 X 20.40 NOZZLE 4 X 42.87 NOZZLE 5 X 20.45 21 NOZELJ/NEI.2516ANNAJ.5 NOZZLE 1 X 40.60 NOZZLE 2 X 40.52 NOZZLE 4 X 77.30 NOZZLE 5 X 91.72 31 NOZELJ/NEI.2516ANNAJ NOZZLE 1 X 40.60 NOZZLE 2 X 41.01 NOZZLE 4 X 82.40 NOZZLE 5 X 77.40 43 NOZELJ/NEI.2516ANNAJ NOZZLE 1 X 50.16 NOZZLE 2 X 50.11 NOZZLE 4 X 110.00 NOZZLE 5 X 100.57	8 GAGE DATA LEFT WING DELTA -.10 DELTA 2 -.10 CWP01Z .0010 .0010 CWP02Z .0010 .0010 CWP03Z .0010 .0010 CWP04Z .0010 .0010 CWP05Z .0010 .0010 CWP06Z .0010 .0010 CWP07Z .0010 .0010 CWP08Z .0010 .0010 CWP09Z .0010 .0010 CWP10Z .0010 .0010 CWP11Z .0010 .0010 CWP12Z .0010 .0010 CWP13Z .0010 .0010 CWP14Z .0010 .0010 CWP15Z .0010 .0010 CWP16Z .0010 .0010 CWP17Z .0010 .0010 CWP18Z .0010 .0010 CWP19Z .0010 .0010 CWP20Z .0010 .0010 CWP21Z .0010 .0010 CWP22Z .0010 .0010 CWP23Z .0010 .0010 CWP24Z .0010 .0010 CWP25Z .0010 .0010 CWP26Z .0010 .0010 CWP27Z .0010 .0010 CWP28Z .0010 .0010 CWP29Z .0010 .0010 CWP30Z .0010 .0010 CWP31Z .0010 .0010 CWP32Z .0010 .0010 CWP33Z .0010 .0010 CWP34Z .0010 .0010 CWP35Z .0010 .0010 CWP36Z .0010 .0010 CWP37Z .0010 .0010 CWP38Z .0010 .0010 CWP39Z .0010 .0010 CWP40Z .0010 .0010 CWP41Z .0010 .0010 CWP42Z .0010 .0010 CWP43Z .0010 .0010 CWP44Z .0010 .0010 CWP45Z .0010 .0010 CWP46Z .0010 .0010 CWP47Z .0010 .0010 CWP48Z .0010 .0010 CWP49Z .0010 .0010 CWP50Z .0010 .0010 CWP51Z .0010 .0010 CWP52Z .0010 .0010 CWP53Z .0010 .0010 CWP54Z .0010 .0010 CWP55Z .0010 .0010 CWP56Z .0010 .0010 CWP57Z .0010 .0010 CWP58Z .0010 .0010 CWP59Z .0010 .0010 CWP60Z .0010 .0010 CWP61Z .0010 .0010 CWP62Z .0010 .0010 CWP63Z .0010 .0010 CWP64Z .0010 .0010 CWP65Z .0010 .0010 CWP66Z .0010 .0010 CWP67Z .0010 .0010 CWP68Z .0010 .0010 CWP69Z .0010 .0010 CWP70Z .0010 .0010 CWP71Z .0010 .0010 CWP72Z .0010 .0010 CWP73Z .0010 .0010 CWP74Z .0010 .0010 CWP75Z .0010 .0010 CWP76Z .0010 .0010 CWP77Z .0010 .0010 CWP78Z .0010 .0010 CWP79Z .0010 .0010 CWP80Z .0010 .0010 CWP81Z .0010 .0010 CWP82Z .0010 .0010 CWP83Z .0010 .0010 CWP84Z .0010 .0010 CWP85Z .0010 .0010 CWP86Z .0010 .0010 CWP87Z .0010 .0010 CWP88Z .0010 .0010 CWP89Z .0010 .0010 CWP90Z .0010 .0010 CWP91Z .0010 .0010 CWP92Z .0010 .0010 CWP93Z .0010 .0010 CWP94Z .0010 .0010 CWP95Z .0010 .0010 CWP96Z .0010 .0010 CWP97Z .0010 .0010 CWP98Z .0010 .0010 CWP99Z .0010 .0010 CWP100Z .0010 .0010 CWP101Z .0010 .0010 CWP102Z .0010 .0010 CWP103Z .0010 .0010 CWP104Z .0010 .0010 CWP105Z .0010 .0010 CWP106Z .0010 .0010 CWP107Z .0010 .0010 CWP108Z .0010 .0010 CWP109Z .0010 .0010 CWP110Z .0010 .0010 CWP111Z .0010 .0010 CWP112Z .0010 .0010 CWP113Z .0010 .0010 CWP114Z .0010 .0010 CWP115Z .0010 .0010 CWP116Z .0010 .0010 CWP117Z .0010 .0010 CWP118Z .0010 .0010 CWP119Z .0010 .0010 CWP120Z .0010 .0010 CWP121Z .0010 .0010 CWP122Z .0010 .0010 CWP123Z .0010 .0010 CWP124Z .0010 .0010 CWP125Z .0010 .0010 CWP126Z .0010 .0010 CWP127Z .0010 .0010 CWP128Z .0010 .0010 CWP129Z .0010 .0010 CWP130Z .0010 .0010 CWP131Z .0010 .0010 CWP132Z .0010 .0010 CWP133Z .0010 .0010 CWP134Z .0010 .0010 CWP135Z .0010 .0010 CWP136Z .0010 .0010 CWP137Z .0010 .0010 CWP138Z .0010 .0010 CWP139Z .0010 .0010 CWP140Z .0010 .0010 CWP141Z .0010 .0010 CWP142Z .0010 .0010 CWP143Z .0010 .0010 CWP144Z .0010 .0010 CWP145Z .0010 .0010 CWP146Z .0010 .0010 CWP147Z .0010 .0010 CWP148Z .0010 .0010 CWP149Z .0010 .0010 CWP150Z .0010 .0010 CWP151Z .0010 .0010 CWP152Z .0010 .0010 CWP153Z .0010 .0010 CWP154Z .0010 .0010 CWP155Z .0010 .0010 CWP156Z .0010 .0010 CWP157Z .0010 .0010 CWP158Z .0010 .0010 CWP159Z .0010 .0010 CWP160Z .0010 .0010 CWP161Z .0010 .0010 CWP162Z .0010 .0010 CWP163Z .0010 .0010 CWP164Z .0010 .0010 CWP165Z .0010 .0010 CWP166Z .0010 .0010 CWP167Z .0010 .0010 CWP168Z .0010 .0010 CWP169Z .0010 .0010 CWP170Z .0010 .0010 CWP171Z .0010 .0010 CWP172Z .0010 .0010 CWP173Z .0010 .0010 CWP174Z .0010 .0010 CWP175Z .0010 .0010 CWP176Z .0010 .0010 CWP177Z .0010 .0010 CWP178Z .0010 .0010 CWP179Z .0010 .0010 CWP180Z .0010 .0010 CWP181Z .0010 .0010 CWP182Z .0010 .0010 CWP183Z .0010 .0010 CWP184Z .0010 .0010 CWP185Z .0010 .0010 CWP186Z .0010 .0010 CWP187Z .0010 .0010 CWP188Z .0010 .0010 CWP189Z .0010 .0010 CWP190Z .0010 .0010 CWP191Z .0010 .0010 CWP192Z .0010 .0010 CWP193Z .0010 .0010 CWP194Z .0010 .0010 CWP195Z .0010 .0010 CWP196Z .0010 .0010 CWP197Z .0010 .0010 CWP198Z .0010 .0010 CWP199Z .0010 .0010 CWP200Z .0010 .0010 CWP201Z .0010 .0010 CWP202Z .0010 .0010 CWP203Z .0010 .0010 CWP204Z .0010 .0010 CWP205Z .0010 .0010 CWP206Z .0010 .0010 CWP207Z .0010 .0010 CWP208Z .0010 .0010 CWP209Z .0010 .0010 CWP210Z .0010 .0010 CWP211Z .0010 .0010 CWP212Z .0010 .0010 CWP213Z .0010 .0010 CWP214Z .0010 .0010 CWP215Z .0010 .0010 CWP216Z .0010 .0010 CWP217Z .0010 .0010 CWP218Z .0010 .0010 CWP219Z .0010 .0010 CWP220Z .0010 .0010 CWP221Z .0010 .0010 CWP222Z .0010 .0010 CWP223Z .0010 .0010 CWP224Z .0010 .0010 CWP225Z .0010 .0010 CWP226Z .0010 .0010 CWP227Z .0010 .0010 CWP228Z .0010 .0010 CWP229Z .0010 .0010 CWP230Z .0010 .0010 CWP231Z .0010 .0010 CWP232Z .0010 .0010 CWP233Z .0010 .0010 CWP234Z .0010 .0010 CWP235Z .0010 .0010 CWP236Z .0010 .0010 CWP237Z .0010 .0010 CWP238Z .0010 .0010 CWP239Z .0010 .0010 CWP240Z .0010 .0010 CWP241Z .0010 .0010 CWP242Z .0010 .0010 CWP243Z .0010 .0010 CWP244Z .0010 .0010 CWP245Z .0010 .0010 CWP246Z .0010 .0010 CWP247Z .0010 .0010 CWP248Z .0010 .0010 CWP249Z .0010 .0010 CWP250Z .0010 .0010 CWP251Z .0010 .0010 CWP252Z .0010 .0010 CWP253Z .0010 .0010 CWP254Z .0010 .0010 CWP255Z .0010 .0010 CWP256Z .0010 .0010 CWP257Z .0010 .0010 CWP258Z .0010 .0010 CWP259Z .0010 .0010 CWP260Z .0010 .0010 CWP261Z .0010 .0010 CWP262Z .0010 .0010 CWP263Z .0010 .0010 CWP264Z .0010 .0010 CWP265Z .0010 .0010 CWP266Z .0010 .0010 CWP267Z .0010 .0010 CWP268Z .0010 .0010 CWP269Z .0010 .0010 CWP270Z .0010 .0010 CWP271Z .0010 .0010 CWP272Z .0010 .0010 CWP273Z .0010 .0010 CWP274Z .0010 .0010 CWP275Z .0010 .0010 CWP276Z .0010 .0010 CWP277Z .0010 .0010 CWP278Z .0010 .0010 CWP279Z .0010 .0010 CWP280Z .0010 .0010 CWP281Z .0010 .0010 CWP282Z .0010 .0010 CWP283Z .0010 .0010 CWP284Z .0010 .0010 CWP285Z .0010 .0010 CWP286Z .0010 .0010 CWP287Z .0010 .0010 CWP288Z .0010 .0010 CWP289Z .0010 .0010 CWP290Z .0010 .0010 CWP291Z .0010 .0010 CWP292Z .0010 .0010 CWP293Z .0010 .0010 CWP294Z .0010 .0010 CWP295Z .0010 .0010 CWP296Z .0010 .0010 CWP297Z .0010 .0010 CWP298Z .0010 .0010 CWP299Z .0010 .0010 CWP300Z .0010 .0010 CWP301Z .0010 .0010 CWP302Z .0010 .0010 CWP303Z .0010 .0010 CWP304Z .0010 .0010 CWP305Z .0010 .0010 CWP306Z .0010 .0010 CWP307Z .0010 .0010 CWP308Z .0010 .0010 CWP309Z .0010 .0010 CWP310Z .0010 .0010 CWP311Z .0010 .0010 CWP312Z .0010 .0010 CWP313Z .0010 .0010 CWP314Z .0010 .0010 CWP315Z .0010 .0010 CWP316Z .0010 .0010 CWP317Z .0010 .0010 CWP318Z .0010 .0010 CWP319Z .0010 .0010 CWP320Z .0010 .0010 CWP321Z .0010 .0010 CWP322Z .0010 .0010 CWP323Z .0010 .0010 CWP324Z .0010 .0010 CWP325Z .0010 .0010 CWP326Z .0010 .0010 CWP327Z .0010 .0010 CWP328Z .0010 .0010 CWP329Z .0010 .0010 CWP330Z .0010 .0010 CWP331Z .0010 .0010 CWP332Z .0010 .0010 CWP333Z .0010 .0010 CWP334Z .0010 .0010 CWP335Z .0010 .0010 CWP336Z .0010 .0010 CWP337Z .0010 .0010 CWP338Z .0010 .0010 CWP339Z .0010 .0010 CWP340Z .0010 .0010 CWP341Z .0010 .0010 CWP342Z .0010 .0010 CWP343Z .0010 .0010 CWP344Z .0010 .0010 CWP345Z .0010 .0010 CWP346Z .0010 .0010 CWP347Z .0010 .0010 CWP348Z .0010 .0010 CWP349Z .0010 .0010 CWP350Z .0010 .0010 CWP351Z .0010 .0010 CWP352Z .0010 .0010 CWP353Z .0010 .0010 CWP354Z .0010 .0010 CWP355Z .0010 .0010 CWP356Z .0010 .0010 CWP357Z .0010 .0010 CWP358Z .0010 .0010 CWP359Z .0010 .0010 CWP360Z .0010 .0010 CWP361Z .0010 .0010 CWP362Z .0010 .0010 CWP363Z .0010 .0010 CWP364Z .0010 .0010 CWP365Z .0010 .0010 CWP366Z .0010 .0010 CWP367Z .0010 .0010 CWP368Z .0010 .0010 CWP369Z .0010 .0010 CWP370Z .0010 .0010 CWP371Z .0010 .0010 CWP372Z .0010 .0010 CWP373Z .0010 .0010 CWP374Z .0010 .0010 CWP375Z .0010 .0010 CWP376Z .0010 .0010 CWP377Z .0010 .0010 CWP378Z .0010 .0010 CWP379Z .0010 .0010 CWP380Z .0010 .0010 CWP381Z .0010 .0010 CWP382Z .0010 .0010 CWP383Z .0010 .0010 CWP384Z .0010 .0010 CWP385Z .0010 .0010 CWP386Z .0010 .0010 CWP387Z .0010 .0010 CWP388Z .0010 .0010 CWP389Z .0010 .0010 CWP390Z .0010 .0010 CWP391Z .0010 .0010 CWP392Z .0010 .0010 CWP393Z .0010 .0010 CWP394Z .0010 .0010 CWP395Z .0010 .0010 CWP396Z .0010 .0010 CWP397Z .0010 .0010 CWP398Z .0010 .0010 CWP399Z .0010 .0010 CWP400Z .0010 .0010 CWP401Z .0010 .0010 CWP402Z .0010 .0010 CWP403Z .0010 .0010 CWP404Z .0010 .0010 CWP405Z .0010 .0010 CWP406Z .0010 .0010 CWP407Z .0010 .0010 CWP408Z .0010 .0010 CWP409Z .0010 .0010 CWP410Z .0010 .0010 CWP411Z .0010 .0010 CWP412Z .0010 .0010 CWP413Z .0010 .0010 CWP414Z .0010 .0010 CWP415Z .0010 .0010 CWP416Z .0010 .0010 CWP417Z .0010 .0010 CWP418Z .0010 .0010 CWP419Z .0010 .0010 CWP420Z .0010 .0010 CWP421Z .0010 .0010 CWP422Z .0010 .0010 CWP423Z .0010 .0010 CWP424Z .0010 .0010 CWP425Z .0010 .0010 CWP426Z .0010 .0010 CWP427Z .0010 .0010 CWP428Z .0010 .0010 CWP429Z .0010 .0010 CWP430Z .0010 .0010 CWP431Z .0010 .0010 CWP432Z .0010 .0010 CWP433Z .0010 .0010 CWP434Z .0010 .0010 CWP435Z .0010 .0010 CWP436Z .0010 .0010 CWP437Z .0010 .0010 CWP438Z .0010 .0010 CWP439Z .0010 .0010 CWP440Z .0010 .0010 CWP441Z .0010 .0010 CWP442Z .0010 .0010 CWP443Z .0010 .0010 CWP444Z .0010 .0010 CWP445Z .0010 .0010 CWP446Z .0010 .0010 CWP447Z .0010 .0010 CWP448Z .0010 .0010 CWP449Z .0010 .0010 CWP450Z .0010 .0010 CWP451Z .0010 .0010 CWP452Z .0010 .0010 CWP453Z .0010 .0010 CWP454Z .0010 .0010 CWP455Z .0010 .0010 CWP456Z .0010 .0010 CWP457Z .0010 .0010 CWP458Z .0010 .0010 CWP459Z .0010 .0010 CWP460Z .0010 .0010 CWP461Z .0010 .0010 CWP462Z .0010 .0010 CWP463Z .0010 .0010 CWP464Z .0010 .0010 CWP465Z .0010 .0010 CWP466Z .0010 .0010 CWP467Z .0010 .0010 CWP468Z .0010 .0010 CWP469Z .0010 .0010 CWP470Z .0010 .0010 CWP471Z .0010 .0010 CWP472Z .0010 .0010 CWP473Z .0010 .0010 CWP474Z .0010 .0010 CWP475Z .0010 .0010 CWP476Z .0010 .0010 CWP477Z .0010 .0010 CWP478Z .0010 .0010 CWP479Z .0010 .0010 CWP480Z .0010 .0010 CWP481Z .0010 .0010 CWP482Z .0010 .0010 CWP483Z .0010 .0010 CWP484Z .0010 .0010 CWP485Z .0010 .0010 CWP486Z .0010 .0010 CWP487Z .0010 .0010 CWP488Z .0010 .0010 CWP489Z .0010 .0010 CWP490Z .0010 .0010 CWP491Z .0010 .0010 CWP492Z .0010 .0010 CWP493Z .0010 .0010 CWP494Z .0010 .0010 CWP495Z .0010 .0010 CWP496Z .0010 .0010 CWP497Z .0010 .0010 CWP498Z .0010 .0010 CWP499Z .0010 .0010 CWP500Z .0010 .0010 CWP501Z .0010 .0010 CWP502Z .0010 .0010 CWP503Z .0010 .0010 CWP504Z .0010 .0010 CWP505Z .0010 .0010 CWP506Z .0010 .0010 CWP507Z .0010 .0010 CWP508Z .0010 .0010 CWP509Z .0010 .0010 CWP510Z .0010 .0010 CWP511Z .0010 .0010 CWP512Z .0010 .0010 CWP513Z .0010 .0010 CWP514Z .0010 .0010 CWP515Z .0010 .0010 CWP516Z .0010 .0010 CWP517Z .0010 .0010 CWP518Z .0010 .0010 CWP519Z .0010 .0010 CWP520Z .0010 .0010 CWP521Z .0010 .0010 CWP522Z .0010 .0010 CWP523Z .0010 .0010 CWP524Z .0010 .0010 CWP525Z .0010 .0010 CWP526Z .0010 .0010 CWP527Z .0010 .0010 CWP528Z .0010 .0010 CWP529Z .0010 .0010 CWP530Z .0010 .0010 CWP531Z .0010 .0010 CWP532Z .0010 .0010 CWP533Z .0010 .0010 CWP534Z .0010 .0010 CWP535Z .0010 .0010 CWP536Z .0010 .0010 CWP537Z .0010 .0010 CWP538Z .0010 .0010 CWP539Z .0010 .0010 CWP540Z .0010 .0010 CWP541Z .0010 .0010 CWP542Z .0010 .0010 CWP543Z .0010 .0010 CWP544Z .0010 .0010 CWP545Z .0010 .0010 CWP546Z .0010 .0010 CWP547Z .0010 .0010 CWP548Z .0010 .0010 CWP549Z .0010 .0010 CWP550Z .0010 .0010 CWP551Z .0010 .0010 CWP552Z .0010 .0010 CWP553Z .0010 .0010 CWP554Z .0010 .0010 CWP555Z .0010 .0010 CWP556Z .0010 .

Printouts of each run sequence set is presented in the appendix of reference 2. The data sets are grouped for a constant Mach number. The first data set within a Mach group is the power-off runs. The second group contains the variable power runs and the third group contains the various elevon deflections.

The base and forebody plume induced data tabulated on the printout sheets were analyzed and developed into math models. The math model is a description of the nominal aerodynamic data and a tolerance model. The math model of the base plume induced aerodynamic characteristics is presented in Section VIII. The math model of the forebody plume induced aerodynamic characteristics is presented in Section IX.

Section VIII

BASE MATH MODEL

A math model of the base plume induced aerodynamic characteristics was developed which can be used in conjunction with the forebody aerodynamic characteristics to evaluate the aerodynamic characteristics of the total space shuttle launch vehicle and each element. Three types of base aerodynamic characteristics were developed. These include 1. SSLV and element base aerodynamic coefficients for Mach numbers from 0.6 to 2.5, 2. SSLV base forces and moments versus altitude up to 160,000 ft. and 3. SSLV and element base coefficient tolerances for Mach numbers from 0.6 to 2.5. The math model consists of a description of the base aerodynamic coefficients at a given Mach number and elevon deflection for various α , β values. Gradients are provided giving the change in the aerodynamic characteristics with the two primary variables that influence the base flow (inboard elevon deflection and SSME power level).

The base aerodynamic math model is limited to the base axial force, normal force and pitching moment. Lateral-directional forces and moments exist on some base components, but no consistent trend could be identified and thus they are included in the base tolerance model. Base coefficients and tolerances for each element are provided for Mach numbers from 0.6 to 2.5. The base aerodynamic coefficient math model is described by the following equation,

$$C_{x_i} = [C_{x_i}]_{\alpha, \beta} + [\partial C_{x_i} / \partial \delta_{EI}] \times \Delta \delta_{EI} + [\partial C_{x_i} / \partial \% \text{ SSME POWER}] \times (\Delta \% \text{ SSME POWER})$$

where $[C_{x_i}]_{\alpha, \beta}$ is a 4x7 matrix for $\alpha = +4, 0, -4, -8$
 $\beta = -6, -4, -2, 0, 2, 4, 6$
 elevon deflection corresponds to close schedule 6
 $i = \text{SSLV, ORBITER, ET, LEFT SRB, RIGHT SRB}$

$\partial C_{x_i} / \partial \delta_{EI}$ Gradient for inboard elevon deflection -
 function of Mach number only
 $i = \text{SSLV, ORBITER, ET}$

$\frac{\partial C_{x_i}}{\partial SSME \text{ POWER}}$ Gradient for percent change in SSME power level - function of Mach number only
i = SSLV, ORBITER

$\Delta\delta_{EI}$ - Change in inboard elevon deflection from math model value to inboard elevon deflection of interest.

$\Delta\%SSME \text{ POWER LEVEL}$ - Change in percent SSME power level from math model value to SSME power level of interest

Typical values of the coefficient $[C_{x_i}]_{\alpha, \beta}$ are presented in Tables 8-1, 8-2, and 8-3 for each element and the total SSLV vehicle. Typical values of the coefficient gradients are presented in Table 8-4.

Base forces and moments have been determined versus altitude using the base coefficient math model. The base force math model is for the total vehicle and uses the following model,

$$\begin{matrix} F \\ M \end{matrix} \Big|_{ALT} = \begin{matrix} F \\ M \end{matrix} \Big|_{\alpha=0} + \begin{bmatrix} \frac{\partial F}{\partial \alpha} \end{bmatrix} \times \alpha + \begin{bmatrix} \frac{\partial F_X}{\partial \delta_{EI}} \end{bmatrix} \Delta\delta_{EI} + \frac{\partial F}{\partial \% \text{ SSME POWER}} \times (\Delta\% \text{ SSME POWER})$$

where:

$\begin{matrix} F \\ M \end{matrix} \Big|_{\alpha=0}$ SSLV base force or moment - function of altitude only

$[\frac{\partial F}{\partial \alpha}]$ Gradient for angle of attack - function of only altitude

$[\frac{\partial F}{\partial \delta_{EI}}]$ Gradient for inboard elevon deflection - function of altitude only

$[\frac{\partial F}{\partial \%SSME \text{ POWER}}]$ Gradient for percent change in SSME power level

α angle of attack

$\Delta\delta_{EI}$ Change in inboard elevon deflection from math model value to inboard elevon deflection of interest

$\Delta\%$ SSME POWER level Change in percent SSME power level from math model value to SSME power level of interest.

Typical values of the base axial force, normal force and pitching moment are presented in Tables 8-5, 8-6, and 8-7. Typical values of the base force partials are presented in Table 8-8.

BASE COEFFICIENT TOLERANCES

Examples of the base coefficient tolerances are presented in Tables 8-9 and 8-10. The coefficient tolerances cover all attitudes and configurations from the base coefficients presented in the math model to flight data and are to a $+3\sigma$ level. The moment tolerances are considered to be only due to force tolerances. The moment tolerance due to the aerodynamic center location uncertainty being a smaller order of magnitude. Examples of the base moment coefficient increment equations are presented in Table 8-10.

The base tolerances include contributions due to 1. test instrumentation uncertainty, 2. simulation parameter uncertainty, 3. Reynolds number characteristics, 4. Model-tunnel testing uncertainties, 5. Pressure integration uncertainties and 6. Math model uncertainties. Each tolerance contribution is assumed independent and therefore the contributions are combined using the RSS technique. The tolerances thus cover the uncertainty from the math model to flight data and are to a $+3\sigma$ level with a Gaussian distribution.

The model instrumentation contribution included the accuracy of the Scanivalve^R calculations. The general accuracy is estimated to be $C_p = \pm 0.013$ for values of C_p in the range of ± 5 . The general uncertainty of the measured pressure coefficients was assumed to be 3%.

The simulation parameter uncertainty was assumed to be due to an uncertainty in the exponent. The estimated uncertainty in the exponent is shown in Figure 5-2. The exponent uncertainty was converted to an error in simulation that generally represented a 10 percent uncertainty in base force coefficients. The Reynolds number-scale uncertainty was obtained using past flight test to wind-tunnel test results. This factor is a judgement factor and includes the differences between the Saturn V and Titan 3C flight and wind tunnel data,

reduced to account for the plume technology program learning curve. This factor also includes a hot flow simulation uncertainty factor. The Reynolds number-scale uncertainty was generally 10% of the nominal base coefficient.

Model configuration uncertainties includes the effect of the support stings that will influence the flow field at angles of sideslip along with uncertainties due to other model configuration inaccuracies that potentially influence the local flow fields. Uncertainties due to model configuration similitude were approximately 7% of the nominal force coefficients.

Integration uncertainties included the potential error involved in the integration technique and represent approximately 3 percent of the nominal force coefficients.

The math model uncertainty included the errors of independent variables in the math model of the base forces and moments. Independent variables not included in the math model of the base forces and moments include nozzle gimbal angle and outboard elevon position.

The technique that was used to develop the SSLV base tolerances was to correlate the SRB and ET base tolerances and RSS those to the orbiter base coefficient tolerance. This procedure was used for the base axial force and normal force coefficients. The SSLV base side force coefficient was obtained by using the RSS technique for each element.

The forebody plume induced aerodynamic characteristics were developed in conjunction with the base plume induced aerodynamic characteristics to allow a complete description of the plume induced characteristics of the Space Shuttle Launch Vehicle. The forebody plume induced aerodynamic characteristics are presented in Section IX.

Table 8-1.

BASE AXIAL FORCE COEFFICIENT

$$M_{\infty} = 1.55 \delta_{e_{10}} = 10/-2$$

% SSME POWER = 109%

ELEMENT	α	β							
		-6	-4	-2	0	2	4	6	
CA-IOL	1.55	-6.	.0685	.0663	.0642	.0625	.0642	.0663	.0685
CA-IOL	1.55	-4.	.0646	.0632	.0616	.0605	.0616	.0632	.0646
CA-IOL	1.55	-2.	.0629	.0616	.0601	.0591	.0601	.0616	.0629
CA-IOL	1.55	0.	.0614	.0602	.0588	.0579	.0588	.0602	.0614
CA-IOL	1.55	2.	.0595	.0583	.0571	.0561	.0571	.0583	.0595
CA-IOL	1.55	4.	.0575	.0563	.0553	.0543	.0553	.0563	.0575
CA-IOL	1.55	6.	.0557	.0546	.0534	.0525	.0534	.0546	.0557
CA-URB	1.55	-6.	.0191	.0194	.0198	.0202	.0198	.0194	.0191
CA-URB	1.55	-4.	.0194	.0197	.0200	.0204	.0200	.0197	.0194
CA-URB	1.55	-2.	.0195	.0197	.0198	.0200	.0198	.0197	.0195
CA-URB	1.55	0.	.0196	.0196	.0196	.0196	.0196	.0196	.0196
CA-URB	1.55	2.	.0194	.0193	.0192	.0191	.0192	.0193	.0194
CA-URB	1.55	4.	.0191	.0189	.0187	.0185	.0187	.0189	.0191
CA-URB	1.55	6.	.0189	.0186	.0182	.0179	.0182	.0186	.0189
CA-ET	1.55	-6.	.0386	.0368	.0349	.0331	.0349	.0368	.0386
CA-ET	1.55	-4.	.0365	.0346	.0326	.0307	.0326	.0346	.0365
CA-ET	1.55	-2.	.0363	.0342	.0321	.0301	.0321	.0342	.0363
CA-ET	1.55	0.	.0361	.0340	.0318	.0297	.0318	.0340	.0361
CA-ET	1.55	2.	.0357	.0336	.0315	.0294	.0315	.0336	.0357
CA-ET	1.55	4.	.0351	.0331	.0312	.0292	.0312	.0331	.0351
CA-ET	1.55	6.	.0346	.0327	.0309	.0290	.0309	.0327	.0346
CA-R	1.55	-6.	.0078	.0067	.0056	.0046	.0039	.0034	.0030
CA-R	1.55	-4.	.0072	.0064	.0055	.0047	.0035	.0025	.0015
CA-R	1.55	-2.	.0064	.0058	.0051	.0045	.0031	.0019	.0007
CA-R	1.55	0.	.0057	.0052	.0047	.0043	.0027	.0014	.0000
CA-R	1.55	2.	.0050	.0046	.0042	.0038	.0022	.0008	.0006
CA-R	1.55	4.	.0044	.0040	.0037	.0033	.0017	.0003	.0011
CA-R	1.55	6.	.0038	.0035	.0031	.0028	.0012	.0002	.0016
CA-L	1.55	-6.	.0030	.0034	.0039	.0046	.0056	.0067	.0078
CA-L	1.55	-4.	.0015	.0025	.0035	.0047	.0055	.0064	.0072
CA-L	1.55	-2.	.0007	.0019	.0031	.0045	.0051	.0058	.0064
CA-L	1.55	0.	.0000	.0014	.0027	.0043	.0047	.0052	.0057
CA-L	1.55	2.	.0006	.0008	.0022	.0038	.0042	.0046	.0050
CA-L	1.55	4.	.0011	.0003	.0017	.0033	.0037	.0040	.0044
CA-L	1.55	6.	.0016	.0002	.0012	.0028	.0031	.0035	.0038

8-5

REPRODUCIBILITY OF THE
ORIGINAL PAGE IS POOR



Table 8-2.

 $M_{\infty} = 1.55$ $\delta_{e_{IO}} = 10/-2$
 % SSME POWER = 109%

BASE NORMAL FORCE COEFFICIENT

ELEMENT	α	β							
		-6	-4	-2	0	2	4	6	
CN-TOL	1.55	-6.	.0135	.0135	.0135	.0135	.0135	.0135	.0135
CN-TOL	1.55	-4.	.0139	.0138	.0138	.0136	.0138	.0138	.0139
CN-TOL	1.55	-2.	.0141	.0138	.0135	.0136	.0136	.0138	.0141
CN-TOL	1.55	0.	.0141	.0139	.0135	.0133	.0135	.0139	.0141
CN-TOL	1.55	2.	.0140	.0138	.0137	.0135	.0137	.0138	.0140
CN-TOL	1.55	4.	.0138	.0138	.0138	.0138	.0138	.0138	.0138
CN-TOL	1.55	6.	.0137	.0138	.0139	.0140	.0139	.0138	.0137
CN-CRB	1.55	-6.	.0131	.0132	.0132	.0133	.0132	.0132	.0131
CN-CRB	1.55	-4.	.0138	.0137	.0136	.0134	.0136	.0137	.0138
CN-CRB	1.55	-2.	.0141	.0138	.0136	.0134	.0136	.0138	.0141
CN-CRB	1.55	0.	.0143	.0140	.0136	.0133	.0136	.0140	.0143
CN-CRB	1.55	2.	.0140	.0137	.0135	.0133	.0135	.0137	.0140
CN-CRB	1.55	4.	.0137	.0135	.0134	.0132	.0134	.0135	.0137
CN-CRB	1.55	6.	.0134	.0133	.0132	.0132	.0132	.0133	.0134
CN-ET	1.55	-6.	.0000	.0000	.0000	.0000	.0000	.0000	.0000
CN-ET	1.55	-4.	.0000	.0000	.0000	.0000	.0000	.0000	.0000
CN-ET	1.55	-2.	.0000	.0000	.0000	.0000	.0000	.0000	.0000
CN-ET	1.55	0.	.0000	.0000	.0000	.0000	.0000	.0000	.0000
CN-ET	1.55	2.	.0000	.0000	.0000	.0000	.0000	.0000	.0000
CN-ET	1.55	4.	.0000	.0000	.0000	.0000	.0000	.0000	.0000
CN-ET	1.55	6.	.0000	.0000	.0000	.0000	.0000	.0000	.0000
CN-K	1.55	-6.	.0001	.0001	.0001	.0001	.0002	.0002	.0003
CN-K	1.55	-4.	.0001	.0001	.0001	.0001	.0001	.0000	-.0000
CN-K	1.55	-2.	-.0000	.0000	.0000	.0001	.0000	-.0000	-.0000
CN-K	1.55	0.	-.0002	-.0001	-.0001	-.0000	.0000	-.0000	-.0000
CN-K	1.55	2.	.0001	.0001	.0001	.0001	.0001	-.0000	-.0001
CN-K	1.55	4.	.0003	.0003	.0003	.0003	.0001	-.0000	-.0002
CN-K	1.55	6.	.0006	.0005	.0005	.0004	.0002	-.0000	-.0003
CN-L	1.55	-6.	.0003	.0002	.0002	.0001	.0001	.0001	.0001
CN-L	1.55	-4.	-.0000	.0000	.0001	.0001	.0001	.0001	.0001
CN-L	1.55	-2.	-.0000	-.0000	.0000	.0001	.0000	.0000	-.0000
CN-L	1.55	0.	-.0000	-.0000	.0000	-.0000	-.0001	-.0001	-.0002
CN-L	1.55	2.	-.0001	-.0000	.0001	.0001	.0001	.0001	.0001
CN-L	1.55	4.	-.0002	-.0000	.0001	.0003	.0003	.0003	.0003
CN-L	1.55	6.	-.0003	-.0000	.0002	.0004	.0005	.0005	.0006

Table 8-3.

$M_\infty = 1.55$ $\delta_{e10} = 10/-2$
 % SSME POWER = 109%

BASE PITCHING MOMENT COEFFICIENT

ELEMENT	α	β							
		-6	-4	-2	0	2	4	6	
CM-IOL	1.55	-6.	-.0063	-.0063	-.0063	-.0062	-.0063	-.0063	-.0063
CM-IOL	1.55	-4.	-.0067	-.0065	-.0064	-.0062	-.0064	-.0065	-.0067
CM-IOL	1.55	-2.	-.0067	-.0065	-.0064	-.0062	-.0064	-.0065	-.0067
CM-IOL	1.55	0.	-.0064	-.0063	-.0061	-.0060	-.0061	-.0063	-.0064
CM-IOL	1.55	2.	-.0065	-.0065	-.0064	-.0063	-.0064	-.0065	-.0065
CM-IOL	1.55	4.	-.0065	-.0066	-.0067	-.0068	-.0067	-.0066	-.0065
CM-IOL	1.55	6.	-.0065	-.0068	-.0070	-.0071	-.0070	-.0068	-.0065
CM-ORB	1.55	-6.	-.0058	-.0059	-.0059	-.0060	-.0059	-.0059	-.0058
CM-ORB	1.55	-4.	-.0063	-.0062	-.0061	-.0060	-.0061	-.0062	-.0063
CM-ORB	1.55	-2.	-.0065	-.0063	-.0062	-.0060	-.0062	-.0063	-.0065
CM-ORB	1.55	0.	-.0066	-.0064	-.0062	-.0060	-.0062	-.0064	-.0066
CM-ORB	1.55	2.	-.0064	-.0063	-.0062	-.0061	-.0062	-.0063	-.0064
CM-ORB	1.55	4.	-.0062	-.0062	-.0062	-.0062	-.0062	-.0062	-.0062
CM-ORB	1.55	6.	-.0060	-.0061	-.0062	-.0063	-.0062	-.0061	-.0060
CM-ET	1.55	-6.	.0000	.0000	.0000	.0000	.0000	.0000	.0000
CM-ET	1.55	-4.	.0000	.0000	.0000	.0000	.0000	.0000	.0000
CM-ET	1.55	-2.	.0000	.0000	.0000	.0000	.0000	.0000	.0000
CM-ET	1.55	0.	.0000	.0000	.0000	.0000	.0000	.0000	.0000
CM-ET	1.55	2.	.0000	.0000	.0000	.0000	.0000	.0000	.0000
CM-ET	1.55	4.	.0000	.0000	.0000	.0000	.0000	.0000	.0000
CM-ET	1.55	6.	.0000	.0000	.0000	.0000	.0000	.0000	.0000
CM-R	1.55	-6.	-.0002	-.0002	-.0002	-.0001	-.0002	-.0002	-.0003
CM-R	1.55	-4.	-.0003	-.0002	-.0002	-.0001	-.0001	-.0001	-.0001
CM-R	1.55	-2.	-.0001	-.0001	-.0001	-.0001	-.0001	-.0001	-.0001
CM-R	1.55	0.	.0002	.0001	.0001	.0000	-.0000	-.0000	.0000
CM-R	1.55	2.	-.0002	-.0002	-.0001	-.0001	-.0001	.0000	.0001
CM-R	1.55	4.	-.0005	-.0004	-.0004	-.0003	-.0001	.0000	.0002
CM-R	1.55	6.	-.0008	-.0007	-.0006	-.0004	-.0002	.0000	.0003
CM-L	1.55	-6.	-.0003	-.0002	-.0002	-.0001	-.0002	-.0002	-.0002
CM-L	1.55	-4.	-.0001	-.0001	-.0001	-.0001	-.0002	-.0002	-.0003
CM-L	1.55	-2.	-.0001	-.0001	-.0001	-.0001	-.0001	-.0001	-.0001
CM-L	1.55	0.	.0000	-.0000	-.0000	.0000	.0001	.0001	.0002
CM-L	1.55	2.	.0001	.0000	-.0001	-.0001	-.0001	-.0002	-.0002
CM-L	1.55	4.	.0002	.0000	-.0001	-.0003	-.0004	-.0004	-.0005
CM-L	1.55	6.	.0003	.0000	-.0002	-.0004	-.0006	-.0007	-.0008

Table 8-4
 BASE COEFFICIENT PARTIALS

		$\partial C_{x_i} / \partial \delta_{EI}$			$[\partial C_{x_i} / \partial \% \text{ SSME POWER}] \times 10$	
MACH		SSLV	ORBITER	ET	SSLV	ORBITER
CA	600	.0025	-.0003	.0028	.0007	.0007
CA	1050	.0040	.0002	.0038	.0010	.0010
CA	1100	.0018	.0003	.0015	.0008	.0008
CA	1250	.0000	.0001	-.0001	.0010	.0010
CA	1400	.0000	.0000	.0000	-.0006	-.0006
CH	600	.0000	.0000	.0000	.0002	.0002
CH	1050	.0001	.0001	.0000	.0005	.0005
CH	1100	.0001	.0001	.0000	.0004	.0004
CH	1250	.0001	.0001	.0000	.0004	.0004
CH	1400	.0001	.0001	.0000	-.0003	-.0003
CM	600	.0000	.0000	.0000	-.0001	-.0001
CM	1050	-.0001	-.0001	.0000	-.0002	-.0002
CM	1100	-.0001	-.0001	.0000	-.0002	-.0002
CM	1250	-.0001	-.0001	.0000	-.0002	-.0002
CM	1400	-.0001	-.0001	.0000	.0001	.0001

8-8

Table 8-6
BASE NORMAL FORCE (LBS)

ALTITUDE (ft)	TOTAL	NOMINAL % SSME POWER LEVEL	ALTITUDE (ft)	TOTAL	NOMINAL % SSME POWER LEVEL
0	0	109	47500	15315	109
5000	18500	109	50000	12685	↓
10000	24966	107	52500	10322	
12000	26867	101	55000	8303	
14000	28381	95	57500	6785	
16000	30163	88.4	60000	5476	
18000	32278	↓	62500	4500	
19000	33678		65000	3900	
20000	36009		67500	2700	
21000	41054		70000	2090	
22000	48096		75000	1175	
23000	50853		80000	391	
24000	51688		85000	-193	
25000	50621		90000	-565	
26000	45343		95000	-791	
28000	40842		↓	100000	
30000	39239	88.4	110000	-1221	
34000	35678	93	120000	-1380	
38000	28850	105	130000	-1384	
40000	25704	109	140000	-1451	
42500	21982	109	150000	-1500	
450000	18546	109	160000	-1400	109

Table 8-7

BASE PITCHING MOMENT (FT. LBS)

ALTITUDE (ft)	PITCHING MOMENT (ft-lbs)	NOMINAL % SSME POWER LEVEL	ALTITUDE (ft)	PITCHING MOMENT (ft-lbs)	NOMINAL % SSM POWER LEVEL
0	0	109	47500	-995473	109
5000	-1220000	109	50000	-828630	↓
10000	-1296826	107	52500	-684740	
12000	-1374159	101	55000	-563750	
14000	-1441528	95	57500	-462600	
16000	-1484908	88.4	60000	-385320	
18000	-1535100	↓	62500	-320000	
19000	-1589046		65000	-250000	
20000	-1701877		67500	-200000	
21000	-1937440		70000	-159200	
22000	-2206003		75000	-38110	
23000	-2218121		80000	-39080	
24000	-2187319		85000	-4825	
25000	-2101904		90000	14130	
26000	-1942585		95000	41395	
28000	-1785366		100000	55800	
30000	-1713072	88.4	110000	72303	
34000	-1515453	93	120000	82300	
38000	-1202968	105	130000	84635	
40000	-1750000	109	140000	88920	
42500	-1458720	109	150000	95000	
45000	-1232990	109	160000	95000	109

Table 8-8
BASE AXIAL FORCE PARTIALS

ALTITUDE (ft)	$\partial AF / \partial \alpha$ (LB/DEG)	$\partial AF / \partial \delta_{EI}$ (LB/DEG)	$\partial AF / \partial \% \text{ SSME POWER}$ (LB/%)
10000	-1331.0	2623.0	73.0
12000	-1361.0	2959.0	71.0
14000	-1536.0	3255.0	62.0
16000	-1823.0	3665.0	43.0
18000	-2454.0	5653.0	26.0
19000	-2667.0	6400.0	23.0
20000	-2716.0	7761.0	31.0
21000	-2021.0	8842.0	107.0
22000	-705.0	9138.0	138.0
23000	1040.0	9098.0	159.0
24000	2461.0	8533.0	167.0
25000	3148.0	6959.0	169.0
26000	2911.0	4350.0	167.0
28000	1627.0	1864.0	142.0
30000	514.0	171.0	158.0
34000	-583.0	87.0	96.0
38000	-1014.0	21.0	-112.0

Table 8-9
IA-119
BASE COEFFICIENT TOLERANCES

$\pm \Delta C_A$

MACH NO.	SSLV	ORB	ET	SRB(1)
.6	.0104	.0031	.0065	.0017
.8	.0107	.0031	.0072	.0015
.9	.0156	.0046	.0107	.0021
.95	.0359	.0088	.0270	.0039
1.05	.0239	.0080	.0161	.0032
1.10	.0169	.0057	.0115	.0022
1.15	.0133	.0046	.0091	.0017
1.25	.0086	.0033	.0060	.0010
1.40	.0062	.0024	.0045	.0006
1.55	.0069	.0032	.0050	.0006
1.80	.0082	.0054	.0050	.0006
2.20	.0078	.0050	.0044	.0008
2.50	.0070	.0040	.0040	.0009

$\pm \Delta C_N^*$

.6	.0029	.0020	.0010	.0006
.8	.0028	.0018	.0009	.0006
.9	.0037	.0026	.0013	.0006
.95	.0065	.0049	.0025	.0006
1.05	.0051	.0045	.0022	.0005
1.10	.0047	.0033	.0016	.0008
1.15	.0037	.0027	.0013	.0006
1.25	.0032	.0019	.0009	.0008
1.40	.0027	.0014	.0007	.0008
1.55	.0030	.0019	.0007	.0008
1.80	.0039	.0032	.0009	.0007
2.20	.0037	.0030	.0010	.0006
2.50	.0032	.0024	.0012	.0005

$*\Delta C_{N_0} = 0.6 \Delta C_{A_0}$

$\pm \Delta C_Y$

.6	.0027	.0025	.0005	.0006
.8	.0022	.0020	.0005	.0005
.9	.0017	.0015	.0006	.0004
.95	.0017	.0015	.0007	.0004
1.05	.0018	.0015	.0009	.0004
1.10	.0019	.0015	.0010	.0004
1.15	.0017	.0015	.0007	.0004
1.25	.0017	.0015	.0006	.0004
1.40	.0016	.0014	.0005	.0004
1.55	.0015	.0012	.0006	.0004
1.80	.0015	.0010	.0008	.0005
2.20	.0017	.0008	.0010	.0008
2.50	.0019	.0006	.0012	.0010

Table 8-10

BASE MOMENT INCREMENTS

The general equations for the element moment increments are

$$\Delta C_M = \Delta C_N \left(\frac{X_N}{L}\right) + \Delta C_A \left(\frac{Z_A}{L}\right)$$

$$\Delta C_{Y_N} = \Delta C_Y \left(\frac{X_{YN}}{L}\right)$$

$$\Delta C_{\ell} = \Delta C_Y \left(\frac{Z_L}{L}\right) + \Delta C_N \left(\frac{Y_L}{L}\right)$$

The SSLV moment increment is determined by the following equations

$$\Delta C_{M_{SSLV}} = \sqrt{(\Delta C_{M_0})^2 + (\Delta C_{M_{ET}} + \Delta C_{M_{RSRB}} + \Delta C_{M_{LSRB}})^2}$$

$$\Delta C_{Y_N \ell_{SSLV}} = \sqrt{(\Delta C_{Y_N \ell_0})^2 + (\Delta C_{Y_N \ell_{ET}})^2 + (\Delta C_{Y_N \ell_{RSRB}})^2 + (\Delta C_{Y_N \ell_{LSRB}})^2}$$

	ORBITER	ET	SRB RIGHT LEFT
$\frac{X_N}{L}$	= .99	.87	1.17
$\frac{Z_A}{L}$	= .31	0.0	0.0
$\frac{X_{YN}}{L}$	= 1.06	0.87	0.195
$\frac{Y_L}{L}$	= 0.0	0.0	1.17
$\frac{Z_L}{L}$	= .27	0.03	0.0

NOTE; L = 1290 INCHES

Section IX

FOREBODY PLUME INDUCED MATH MODEL

The nominal forebody plume induced aerodynamic characteristics were small except on the Orbiter fuselage, inboard elevon and the vertical tail. Math models were thus developed for the SSLV, Orbiter, the inboard elevon hinge moment and the vertical tail. The SSLV and Orbiter normal force, pitching moment and inboard elevon hinge moment was formulated into the following math model.

$$\begin{matrix} C_N \\ C_M \\ C_{H_{e_I}} \end{matrix} = C_{N \alpha-\beta \text{ MATRIX}} + \begin{bmatrix} \partial C_N / \partial \delta_{EI} \\ \alpha-\beta \\ \text{MATRIX} \\ > \\ < \end{bmatrix} \times \Delta \delta_{EI} + \begin{bmatrix} \partial C_N / \partial \delta_{EO} \\ > \\ < \end{bmatrix} \times \Delta \delta_{EO} \alpha-\beta \text{ MATRIX}$$

where C_N is a 4x7 matrix for $\alpha = +4, 0, -4, -8$
 $\beta = -6, -4, -2, 0, 2, 4, 6$
 elevon deflection corresponds to close schedule 6
 $\partial C_N / \partial \delta_{EI}$ is a 4x7 matrix for $\alpha = +4, 0, -4, -8$
 $\beta = -6, -4, -2, 0, 2, 4, 6$
 > gradient for inboard elevon deflections > nominal
 < gradient for inboard elevon deflections < nominal
 $\partial C_N / \partial \delta_{EO}$ is a 4.7 matrix for $\alpha = +4, 0, -4, -8$
 $\beta = -6, -4, -2, 0, 2, 4, 6$
 > gradient for outboard elevon deflections > nominal
 < gradient for outboard elevon deflections < nominal

$\Delta \delta_{EI}$ - change in inboard elevon deflection from nominal value to inboard elevon deflection of interest.

$\Delta \delta_{EO}$ - change in outboard elevon deflection from nominal value to outboard elevon deflection of interest.

Typical values of SSLV and Orbiter plume induced forebody normal force coefficients are presented in Table 9-1.

The orbiter normal force and pitching moment math models were derived from the results of the pressure integration of the power-delta pressure coefficients. The orbiter data used to derive the math model is presented in the tabulated data in the Appendix - Section 9 (Forebody Pressure Integration) of the printout sheet (see Section VII). The SSLV and Orbiter math models are identical since only the orbiter plume effects are included in the math model.

The hinge moment math model was derived from the left wing gage data, although the data is presented for the right wing. A comparison of the left wing gage data and the right wing pressure integration data was made to evaluate the best data to use and the gage data had the most consistent trend with changes in attitude and configuration. The left wing gage data used to develop the hinge moment math model is presented in the tabulated data in the appendix in Section 8 (GAGE DATA) of the printout sheet (see Section VII).

The vertical tail shear force, bending moment and torsion moment coefficient were formulated into the following math model

$$C_v = [C_{v_{\alpha-\beta}}]_{Matrix}$$

where

$$[C_{v_{\alpha-\beta}}]_{Matrix} \text{ is a } 4 \times 7 \text{ matrix for } \alpha = +4, 0, -4, -8$$

$$\beta = -6, -4, -2, 0, 2, 4, 6$$

for elevon deflections noted on the table.

C_{YV} , vertical tail power delta shear force coefficient

C_{BV} , vertical tail power delta bending moment coefficient

C_{TV} , vertical tail power delta torsion moment coefficient

The vertical tail shear force math model includes only the $\alpha-\beta$ matrix at the nominal elevon deflection. No influence of elevon deflections are included. The vertical tail power induced shear force, bending moment, and torsion moment coefficients were developed into table format. A typical example is presented in Table 9-2.

The vertical tail math model was derived from the integration of the vertical tail pressure data presented in the tabulated data in the appendix in Section 9 (Forebody Pressure Integration) of the printout sheet (see Section VII).

FOREBODY COEFFICIENT TOLERANCES

Forebody tolerances have been developed for all forebody elements and components. As mentioned above, only the Orbiter, inboard elevon hinge moment and the vertical tail had measurable plume induced aerodynamic changes that could be effectively modeled. The other elements and components have zero nominal math model plume induced aerodynamic characteristics. Tolerances have been developed for all element and components, however, to account for all possible variations in plume induced aerodynamic characteristics. The forebody element and component force coefficient tolerances are presented as tabled values that are the $\pm 3\sigma$ variation of the nominal coefficient. The $\pm 3\sigma$ variation covers the potential variation of the coefficient from the math model results to expected flight data values.

Examples of the SSLV and element force coefficient tolerances are presented in Table 9-3. The moment increment equations are presented in Table 9-4. Examples of the component force coefficient tolerances and moment equations are presented in Tables 9-5 and 9-6. The moment tolerances require using equations that include the force coefficient tolerances along with the nominal aerodynamic center in conjunction with the nominal forebody power delta (when $\neq 0$) times the aerodynamic center tolerance.

The forebody tolerances include contributions due to 1. test instrumentation uncertainty, 2. simulation parameter uncertainty, 3. Reynolds number characteristics, 4. Model-tunnel testing uncertainties, 5. Pressure integration uncertainties and 6. Math model uncertainties. Each tolerance contribution is assumed independent and therefore the contributions are combined using the RSS technique. The tolerances thus cover the uncertainty from the math model to flight data and are to a $\pm 3\sigma$ level with a Gaussian distribution.

The forebody coefficients are determined using power delta's. Thus the instrumentation accuracy includes two independent measurements that are combined

by the RSS techniques. The instrumentation accuracy for a single measurement is estimated to be 3 percent. Thus two measurements would be 4.3 percent. The general uncertainty in the nominal forebody force coefficient due to instrumentation uncertainty was estimated at 50 percent of the calculated nominal forebody coefficient. The similarity parameter uncertainty was estimated to be 30 percent of the nominal, Reynolds number and scale effect was estimated to be 100 percent of the nominal, model uncertainties were estimated to be 30 percent of the nominal, integration uncertainties at 30 percent of the nominal and math model uncertainties were estimated at 20 percent of the nominal value. The net RSS tolerance value for the forebody coefficients are large compared to the nominal math model values. This is because the nominal math model force coefficients are small. If the math model is not used the tolerance would be approximately double the values presented and it was determined that forebody tolerances approach double the values would be excessive.

Portions of the forebody have zero nominal plume induced aerodynamic force coefficients in the math model although specific computed values have been determined and are listed in the tabulated data in the appendix (see Section VII). The tolerance analysis discussed above considered the nominal values calculated although the math model nominal force coefficients are zero.

Table 9-1. SSLV AND ORBITER POWER DELTA - NORMAL FORCE COEFFICIENT - FOREBODY

MACH	$\delta_{e_{10}}$	α	β						
			-6	-4	-2	0	+2	+4	+6
1.10	10/9	4	+0.0063	+0.0061	+0.0058	+0.0056	+0.0058	+0.0061	+0.0063
		0	+0.0085	+0.0080	+0.0070	+0.0053	+0.0070	+0.0080	+0.0085
		-4	+0.0090	+0.0085	+0.0080	+0.0075	+0.0080	+0.0085	+0.0090
		-8	+0.0096	+0.0093	+0.0090	+0.0088	+0.0090	+0.0093	+0.0096
1.15	10/5	4	+0.0080	+0.0077	+0.0057	+0.0053	+0.0057	+0.0077	+0.0080
		0	+0.0079	+0.0075	+0.0057	+0.0052	+0.0057	+0.0075	+0.0079
		-4	+0.0080	+0.0077	+0.0072	+0.0070	+0.0072	+0.0077	+0.0080
		-8	+0.0095	+0.0092	+0.0081	+0.0075	+0.0081	+0.0092	+0.0095
1.25	10/-2	4	+0.0043	+0.0048	+0.0053	+0.0058	+0.0053	+0.0048	+0.0043
		0	+0.0055	+0.0059	+0.0063	+0.0067	+0.0063	+0.0059	+0.0055
		-4	+0.0070	+0.0070	+0.0071	+0.0071	+0.0071	+0.0070	+0.0070
		-8	+0.0093	+0.0096	+0.0099	+0.0102	+0.0099	+0.0096	+0.0093
1.40	10/-2	4	+0.0060	+0.0056	+0.0051	+0.0047	+0.0051	+0.0056	+0.0060
		0	+0.0060	+0.0056	+0.0051	+0.0047	+0.0051	+0.0056	+0.0060
		-4	+0.0068	+0.0070	+0.0073	+0.0075	+0.0073	+0.0070	+0.0068
		-8	+0.0090	+0.0101	+0.0105	+0.0108	+0.0105	+0.0101	+0.0096

Table 9-2. VERTICAL TAIL SIDE FORCE POWER DELTA

MACH.	δe_{10}	α	β						
			-6	-4	-2	0	+2	+4	+6
.6	10/9	4	+0.0339	+0.0226	+0.0113	+0.0000	-0.0113	-0.0226	-0.0339
		0	+0.0278	+0.0185	+0.0093	+0.0000	-0.0093	-0.0185	-0.0278
		-4	+0.0302	+0.0201	+0.0100	+0.0000	-0.0100	-0.0201	-0.0302
		-8	+0.0249	+0.0166	+0.0083	+0.0000	-0.0083	-0.0166	-0.0249
.8	10/9	4	+0.0129	+0.0086	+0.0043	+0.0000	-0.0043	-0.0086	-0.0129
		0	+0.0080	+0.0053	+0.0026	+0.0000	-0.0026	-0.0053	-0.0080
		-4	+0.0014	+0.0010	+0.0005	+0.0000	-0.0005	-0.0010	-0.0014
		-8	+0.0015	+0.0010	+0.0005	+0.0000	-0.0005	-0.0010	-0.0015
.9	10/9	4	+0.0170	+0.0113	+0.0057	+0.0000	-0.0057	-0.0113	-0.0170
		0	+0.0170	+0.0113	+0.0057	+0.0000	-0.0057	-0.0113	-0.0170
		-4	+0.0210	+0.0140	+0.0070	+0.0000	-0.0070	-0.0140	-0.0210
		-8	+0.0158	+0.0105	+0.0053	+0.0000	-0.0053	-0.0105	-0.0158
.95	10/9	4	+0.0689	+0.0459	+0.0230	+0.0000	-0.0230	-0.0459	-0.0689
		0	+0.0654	+0.0436	+0.0218	+0.0000	-0.0218	-0.0436	-0.0654
		-4	+0.0615	+0.0410	+0.0205	+0.0000	-0.0205	-0.0410	-0.0615
		-8	+0.0566	+0.0377	+0.0188	+0.0000	-0.0188	-0.0377	-0.0566
1.05	10/9	4	+0.0369	+0.0246	+0.0123	+0.0000	-0.0123	-0.0246	-0.0369
		0	+0.0340	+0.0227	+0.0113	+0.0000	-0.0113	-0.0227	-0.0340
		-4	+0.0279	+0.0186	+0.0093	+0.0000	-0.0093	-0.0186	-0.0279
		-8	+0.0315	+0.0210	+0.0105	+0.0000	-0.0105	-0.0210	-0.0315

9-6

Table 9-3

FOREBODY FORCE COEFFICIENT TOLERANCES - SSLV AND ELEMENTS

MACH NO.	$\pm\Delta C_A$			
	SSLV	ORB	ET	SRB(1)
.6	.0038	.0010	.0010	.0025
.8	.0038	.0010	.0010	.0025
.9	.0038	.0010	.0010	.0025
.95	.0052	.0012	.0012	.0035
1.05	.0037	.0017	.0017	.0020
1.1	.0035	.0015	.0015	.0020
1.15	.0035	.0015	.0015	.0020
1.25	.0045	.0014	.0014	.0025
1.40	.0040	.0013	.0013	.0025

MACH NO.	$\pm\Delta C_N$			
	SSLV	ORB	ET	SRB(1)
.6	.0068	.0060	.0030	.0010
.8	.0077	.0070	.0030	.0010
.9	.0094	.0080	.0040	.0020
.95	.0101	.0080	.0050	.0025
1.05	.0099	.0080	.0055	.0015
1.1	.0089	.0070	.0050	.0015
1.15	.0067	.0050	.0040	.0015
1.25	.0055	.0030	.0030	.0025
1.40	.0079	.0030	.0020	.0050

MACH NO.	$\pm\Delta C_Y$			
	SSLV	ORB	ET	SRB(1)
.6	.0083	.0080	.0005	.0015
.8	.0083	.0080	.0005	.0015
.9	.0093	.0090	.0006	.0015
.95	.0109	.0100	.0007	.0030
1.05	.0098	.0080	.0010	.0040
1.10	.0093	.0060	.0010	.0050
1.15	.0082	.0040	.0008	.0050
1.25	.0064	.0030	.0006	.0040
1.40	.0052	.0030	.0006	.0030

Table 9-4

FOREBODY MOMENT INCREMENT EQUATIONS - SSLV AND ELEMENTS

ELEMENTS
$$\Delta C_M = \sqrt{\left[\Delta C_N \left(\frac{X_N}{L} \right)^2 + \left[C_N \left(\frac{\Delta X_N}{L} \right) \right]^2 + \left[\Delta C_A \left(\frac{Z_A}{L} \right) \right]^2}$$

$$\Delta C_{YN} = \sqrt{\left[\Delta C_Y \left(\frac{X_{YN}}{L} \right)^2 + \left[\Delta C_A \left(\frac{Y_{ZL}}{L} \right) \right]^2}$$

$$\Delta C_{ZL} = \sqrt{\left[\Delta C_Y \left(\frac{Z_L}{L} \right)^2 + \left[\Delta C_N \left(\frac{Y_L}{L} \right) \right]^2}$$

SSLV TYPICAL
$$\Delta C_{M_{SSLV}} = \sqrt{(\Delta C_{M_0})^2 + (\Delta C_{M_{ET}})^2 + (\Delta C_{M_{RSRB}})^2 + (\Delta C_{M_{LSRB}})^2}$$

MACH	ORB							ET						
	$\frac{X_N}{L}$	$\frac{\Delta X_N}{L}$	$\frac{X_{YN}}{L}$	$\frac{Z_L}{L}$	$\frac{Y_{ZL}}{L}$	$\frac{Y_L}{L}$	$\frac{Z_A}{L}$	$\frac{X_N}{L}$	$\frac{\Delta X_N}{L}$	$\frac{X_{YN}}{L}$	$\frac{Z_L}{L}$	$\frac{Y_{ZL}}{L}$	$\frac{Y_L}{L}$	$\frac{Z_A}{L}$
.6	.92	.03	.98	.42	0	0	.26	.7	0	.7	.03	.03	.03	.03
.8	.93	.03	.94	.42	0	0	.26	.7	0	.7	.03	.03	.03	.03
.9	.96	.03	1.02	.43	0	0	.26	.8	0	.8	.03	.03	.03	.03
.95	1.01	.03	1.03	.44	0	0	.26	.8	0	.8	.03	.03	.03	.03
1.05	.95	.04	1.02	.45	0	0	.26	.8	0	.8	.03	.03	.03	.03
1.10	.96	.03	1.01	.45	0	0	.26	.8	0	.8	.03	.03	.03	.03
1.15	.97	.02	1.0	.44	0	0	.26	.8	0	.8	.03	.03	.03	.03
1.25	.98	.02	1.0	.44	0	0	.26	.8	0	.8	.03	.03	.03	.03
1.40	.99	.02	1.0	.44	0	0	.26	.8	0	.8	.03	.03	.03	.03

MACH	SRB RIGHT LEFT						
	$\frac{X_N}{L}$	$\frac{\Delta X_N}{L}$	$\frac{X_{YN}}{L}$	$\frac{Z_L}{L}$	$\frac{Y_{ZL}}{L}$	$\frac{Y_L}{L}$	$\frac{Z_A}{L}$
.6	1.15	0	1.15	0	.194	.194	.02
.8	1.15	0	1.15	0	.194	.194	.02
.9	1.15	0	1.15	0	.194	.194	.02
.95	1.14	0	1.14	0	.194	.194	.02
1.05	1.14	0	1.14	0	.194	.194	.02
1.10	1.13	0	1.13	0	.194	.194	.02
1.15	1.10	0	1.10	0	.194	.194	.02
1.25	1.10	0	1.10	0	.194	.194	.02
1.40	1.10	0	1.10	0	.194	.194	.02

NOTE: L = 1290 INCHES

Table 9-5

FOREBODY FORCE TOLERANCES — COMPONENTS

WING TOLERANCES		VERTICAL TAIL TOLERANCES
MACH	$\pm\Delta CNW$	$\pm\Delta CYV$
.6	.0050	.010
.8	.0050	.010
.9	.0050	.030
.95	.0050	.030
1.05	.0060	.030
1.10	.0065	.010
1.15	.0060	.008
1.25	.0040	.010
1.40	.0040	.006

Table 9-6

FOREBODY MOMENT EQUATIONS — COMPONENTS

WING

$$\Delta C_{BW} = \Delta C_{NW} \left(\frac{y_w}{b} \right)$$

$$\Delta C_{TW} = \Delta C_{NW} \left(\frac{x_w}{c} \right)$$

VERTICAL TAIL

$$\Delta C_{BV} = \sqrt{\left[\Delta C_{YV} \left(\frac{Z_V}{L} \right)^2 + C_{YV} \left(\frac{\Delta Z_V}{L} \right)^2 \right]}$$

$$\Delta C_{TV} = \sqrt{\left[\Delta C_{YV} \left(\frac{X_V}{L} \right)^2 + C_{YV} \left(\frac{\Delta X_V}{L} \right)^2 \right]}$$

HINGE MOMENT

$$\Delta CHEI = \Delta CHEI$$

$$\Delta CHEO = \Delta CHEO$$

MACH	WING ¹			VERTICAL ²			+ΔCHEI	+ΔCHEO
	$\frac{y_w}{b}$	$\frac{x_w}{c}$	$\frac{Z_V}{L}$	$\frac{\Delta Z_V}{L}$	$\frac{X_V}{L}$	$\frac{\Delta X_V}{L}$		
.6	.091	-.22	.60	.20	.34	.10	.0050	.0020
.8	.095	-.20	.75	.20	.33	.10	.0050	.0015
.9	.098	-.27	.42	.20	.59	.17	.0100	.0040
.95	.105	-.26	1.10	.25	.84	.20	.0130	.0100
1.05	.110	-.26	.72	.30	.51	.25	.0100	.0030
1.10	.100	-.28	.91	.30	.81	.20	.0080	.0010
1.15	.110	-.32	.63	.20	.87	.20	.0070	.0010
1.25	.110	-.33	.34	.15	.78	.15	.0050	.0010
1.40	.110	-.32	.45	.30	.40	.10	.0050	.0010

¹ For Wing

b = 936.68"
c = 474.81"

² Vertical

L = 199.8 in.

Section X

CONCLUSIONS

The data from tests IA119 and IA138 resulted in an appreciable amount of good plume induced aerodynamic data. Problems with the data were very limited and the power off data compares very good with other tests.

The major independent variables that change the plume induced aerodynamic characteristics are angle of attack, angle of sideslip, inboard elevon deflection and SRB and SSME power level. Plume induced aerodynamic characteristics and their tolerances for the base and forebody have been developed into math models compatible with the forebody math models.

A math model of the plume induced aerodynamic coefficients for the base was developed for the Mach number range from 0.6 to 2.5. Data tables of these coefficients have been provided in G.E. mass format for computer simulation. A math model of the forces and moments for the base was also developed covering the portion of ascent flight up to 160,000 ft. The data tables for the base force math model was also provided in G.E. mass format. A math model of the forebody plume induced aerodynamic coefficients was also developed and the data tables provided in G.E. mass format. The tolerances for the plume induced aerodynamic coefficients and the tolerance math models for the base and forebody were developed and data tables provided in G.E. mass format.

The plume induced aerodynamic characteristics of the orbiter base are the result of a complicated integration of pressure coefficients and power delta pressure coefficients. These aerodynamic characteristics were developed such that when combined with the forebody data they produce the proper total vehicle aerodynamic characteristics.

The ET base plume induced axial force is larger than previous analyses have predicted, however, it is felt that the present results are consistent and representative of the ET base pressure environment.

The plume induced near field (base environment) and far field (orbiter forebody wing and hinge moment data) had good consistent trends when plotted versus the plume similarity parameter. The consistency of the data for both the near field and far field added confidence in the similarity parameter used.

Section XI
RECOMMENDATIONS

A computer program was developed to integrate the pressure data for all elements and components and tabulate the results and the results of the gage data. The tabulated results and plotted power variation data represent approximately 2000 computer printout pages. Time did not permit an extensive analysis of all the data. It is recommended that additional analyses be conducted of the vertical tail data, wing data, inboard hinge moment data and orbiter fuselage data.

It is also recommended that the IA119 and IA138 test results be reevaluated using the new similarity parameters.

Section XII

REFERENCES

1. Boyle, W. W. and Conine, B. H., "Space Shuttle Plume Simulation/Application - Final Report Results and Math Model, NSI Report TR-230-1962, dated 15 July 1978.
2. Boyle, W. W., Conine, B. H., and Bell, G., "Space Shuttle Plume Simulation/Application - Final Report Results and Math Model - Supersonic Data", NSI Report TR-230-1963, dated 15 May 1979.
3. Dziubala, T. J. and Marroquin, J., "Pretest Information for Test IA119 of the 0.020-Scale 88-OTS Configuration 140 C (Modified) Integrated Space Shuttle Vehicle Test-Plume Model in the NASA/ARC UP WT 11 by 11 Foot Leg for Determination of Aspiration-Induced Effects", Document SD-77-SH-0196, Rockwell International, Space Division, September 20, 1977.
4. Marroquin, J., "Pretest Information for Test IA138 of the 0.010-Scale 75-OTS Jet Plume Space Shuttle Model in the 9x7-Foot Leg of the NASA/ARC Unitary Plan Wind Tunnel", Document SD78-SH-0133, Rockwell International, Space Division, 12 June 1978.
5. Harden, R. B. and Campbell, J. R. II, "Pretest Information for Test IA19 of the 0.02 Scale 88-OTS Jet Plume Space Shuttle Model in the 11x11 Foot Leg of the NASA/ARC Unitary Plan Wind Tunnel", Document 5074-SH-0276, Rockwell International Space Division, dated 9 March 1974.
6. Andrews, C. D., "MSFC Input for RI/SD SSLV Wind Tunnel Tests IA119/IA138 NASA Memo ED32-77-13, dated 23 February 1977.
7. Boyle, W. W., "Plume Technology Program Base Pressure Similarity Parameters", NSI Memo M-9230-76-45, dated July 1976.
8. Sims, Joseph L., "Plume Simulation Technology", MSFC Systems Dynamics Laboratory Viewgraph Presentation, January 1979.